International Journal of Advanced Research in Physical Science (IJARPS)
Volume 11, Issue 12, 2024, PP 3-31
ISSN (Online)-2349-7882
www.arcjournals.org

The Effect of Low Atomic Number Fillters on the Flattening Filters free photon Beamin in Radiotherapy

Hadeel Mohammed Saleh Alfrihidi*, Dr. Hussein Abdulrahman Albarakaty

Saudi Arabia Kingdom

Corresponding Author:** ***Hadeel Mohammed Saleh Alfrihidi, *Saudi Arabia Kingdom*

Abstract: *This study aimed to improve the flattening filter-free beam quality using filters made from low-z materials like steel and aluminum using Monte Carlo simulations. A 6 MV True-Beam linear accelerator was simulated using BEAMnrc user code based on the electron gamma shower MC method. Varian Medical Systems and the International Atomic Energy Agency provided phase-space files, and we used them as radiation sources in the simulations for the FFF and FF, respectively. These phase space files include information regarding the passage of the beam in the linac head and scored 27.88 cm from the target, just above the jaws. The passage of the beam was simulated downstream the jaws and scored 100 cm from the target. To study the effect of low-z material filters, steel and Al filters with various thicknesses were added under the jaws. For comparison, the FF beam was simulated using a similar configuration. A Beam data processor user code was used to derive the energy spectra of the beams using the phase space files generated by BEAMnrc. After that, the dose distribution resulting from these beams was simulated in a homogeneous water phantom using the DOSXYZnrc user code. The dose profile was evaluated according to the surface and percentage depth doses. The energy spectra of the beams show that the FFF beam is softer than the FF beam. Adding an Al and steel filter with the FFF beam will make the beam harder. Moreover, steel and aluminum filters decreased the surface dose. On the other hand, adding steel and Al filters to the FFF beam reduces the dose rate of the FFF beam. However, their effect on the dose rate is less than the tungsten FF, which reduces the dose rate more. Briefly, filters from low-z material decrease the surface dose and increase the dose at depth, enabling the delivery of large doses to deep tumors with a minimal skin dose.*

Keywords: *Dose rate, Energy spectrum, Flattening filter free, Monte Carlo, Radiotherapy, Surface dose.*

1. INTRODUCTION

High-energy radiation is used in radiotherapy (RT) to stop the growth and spreading of cancer cells and to kill them. The journey commences with a Computrized Tomography (CT) simulation. This non-invasive imaging technique generates detailed three-dimensional (3D) anatomical maps of the target region and surrounding structures. The CT scan serve as a crucial roadmap, guiding the subsequent treatment planning and ensuring accurate radiation delivery.

The function of the FF is to make the beam intensity uniform across the field. Various linear accelerators (Linacs) are appropriate for therapeutic purposes. Specific devices provide X-rays with different energy spectra, while others produce an electron beam. In X-ray mode, a typical linac has a flattening filter (FF) positioned between the primary collimator and the ionization chamber.

Recently, linacs without FF have been produced as a new technique known as flattening filter free (FFF) beams. The therapeutic effects of these radiation beams are widely recognized. One of these advantages is increasing the dose rate while decreasing the treatment duration [1]. This is essential for all patients but is especially essential in situations requiring larger doses, such as those involving some types of stereotactic radiosurgery (SRS), intensity-modulated radiation therapy (IMRT), or volumetric modulated arc therapy (VMAT) procedures. On the other hand, the FFF beam has a higher surface dose than the FF beam, which is considered a disadvantage [1], [2].

Therfore, how the beam exits the collimator is the leading cause of the decrease in treatment duration. In conventional linacs, a beam passes through the FF then leaves. Since many of these filters are made of tungsten, a substance with a high atomic number, photons interacted with it, resulting in a significant loss of intensity. In contrast, the absence of this absorber in the beam path causes a higher intensity of radiation to pass through the collimator for FFF beams. Therefore, when the FFF modality is selected, more radiation leaves the equipment. In this sense, using FFF beams in therapeutic procedures quickly expands [3], [4].

With the growing availability and utilization of FFF beams, my research aims to enhance the therapeutic outcomes of FFF beams by decreasing the surface dose while ensuring a higher dose rate. This study uses a Monte Carlo (MC) simulation technique to investigate how adding low-z filters into the FFF beam's path will affect the beam quality, surface dose, and dose rate. The main objective of this study is to study the effect of adding filters from low-z material on improving the RT outcomes of the FFF beam and this is done by

- Simulate the the FF, FFF, and FFF with low-z filter beams using BEAMnrc user code.
- To analyze the phase space (phsph) files generated by BEAMnrc user code using BEAMdp (Beam data processor).
- Simulate the dose distribution of all beam configurations using the DOSXYZnrc user code.
- To compare the dosimetric characteristics of the FF, FFF, and FFF with low-z filter beams such as beam quality and surface dose.

2. BACKGROUND

2.1. History of Radiotherapy

Before discovering the ionizing particle beams, medicine had limited cancer treatment options. The situation quickly improved and changed once Wilhelm Conrad Roentgen discovered X-rays in 1895. In rhat year, Antoine Henri Becquerel began researching natural radiation sources and studying radioactivity phenomena. Maria Sklodowska-Curie and her husband, Pierre Curie, discovered radium as a radiation source in 1898. After that, there was a rise in the number of studies reporting the use of X-rays and radium in medicine. Skin cancers were the most often treated on account of radiation's low penetration into tissue. Coolidge invented a new machine that emits higher-intensity X-rays in the 1910s to treat deeper cancers [5]. Between 1920 and 1950, there was a distinguishing progress in the field of RT. The most noticeable discoveries in the following era were radium-based interstitial irradiation and the creation of super-voltage x-ray tubes capable of delivering energy ranging from 50 to 200 keV. The studies performed during the next three decades also focused on creating more creative radio-therapeutic devices capable of treating tumors in the deep tissues. This period is also known as the megavoltage era. However, the progress and discoveries continue more and more until the present day [6].

2.2. What is Radiotherapy

RT is an active therapeutic technique for tumors. RT attacks tumors by using X-rays, gamma rays, and other forms of radiation that can ionize atoms. Radiation destroys cells by disintegrating molecules and causing chemical reactions that harm living cells. Sometimes, cells are killed instantly; other times, particular components of cells, such as their deoxyribonucleic (DNA), are destroyed, impairing the cell's reproduction capacity.

Although radiation causes harm to both cancerous and healthy cells, the purpose of RT is to increase radiation dose to cancer cells while reducing exposure to healthy cells surrounding it or in the path of radiation. Healthy cells can generally mend themselves faster and maintain their normal function than cancer cells [7].

2.3. Radiation Basics

2.3.1.Radiation Types

There are two primary forms of radiation, each with a distinct set of properties and effects.

- X-rays and Gamma-rays represent electromagnetic radiation. It is a packet of energy traveling through space.
- Electrons, neutrons, and protons represent particle radiation. They travel as particles in matter.

RT can use all these types, but the most conventional modality is X-rays produced in a Linac machine, which was used in the current study [8].

2.3.2.Radiation Delivery

There are two methods for delivering radiation to the tumor. First, external beam radiation is delivered from outside the body by focusing high-energy rays (photons, protons, or particle radiation) on the tumor's position. Second, Internal radiation, also known as brachytherapy, delivers a high dose of radiation from inside the body near the cancer [7]. Figure2.1 shows the external and internal RT in the treatment of cancer.

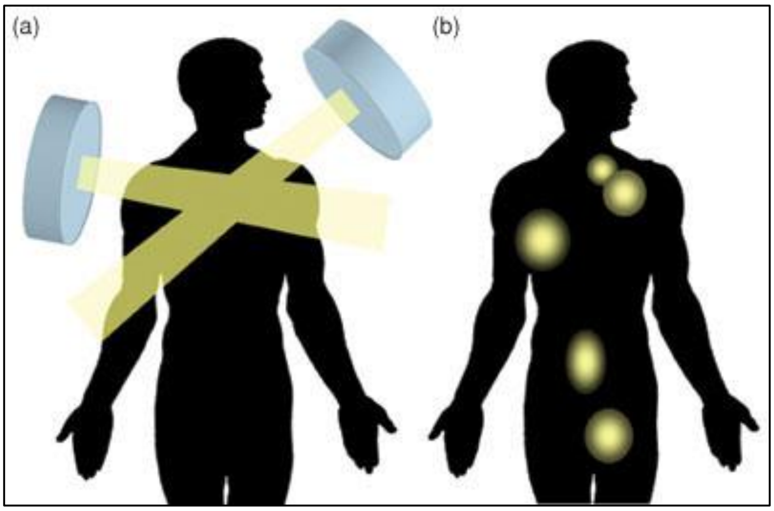

Figure2.1. *Two main types of delivering radiation to patient* ***a.****External radiation therapy* ***b.*** *Internal radiation therapy.*

2.4. Linac machine

2.4.1.Overview

The Linac produces and delivers high-energy rays directed toward the tumor cell and a specific region near the tumor. Different types of these machines generate different kinds of energy. For example, the True beam machine produces 6,10,15, and 18 MV photon energies and is used to produce electron energies. Moreover, Clinic 600C/CD has photon beams with energies of 4MV or 6MV, but it does not produce electron energies [8].

Medical linacs have progressed and are now used for their flexible energy range and excellent dose rates. In a linac, photon energies vary from 4 to 23 MV. Some are used to treat tumors on the outside of the body. Others are focused on treating tumors that have spread throughout the body [8].

2.4.2.Linac's working principle

Linac is a machine that accelerates charged particles in a tube-shaped structure called the accelerator waveguide using high radio-frequency electromagnetic waves. The following steps describe these process, from producing the electron beam until reaching the Linac's head.

Figure2.2 illustrates different parts used for the beam generation in the stand of the linac machine.

- The modulator contains the pulse-forming network connected to a direct current (DC) power supply.
- A pulse with a high voltage reaches the magnetron or klystron (power source), which provides a high-frequency microwave.
- At the same time, the pulse reaches the electron gun. The electron gun is a cathode that acts as a source of electrons.
- After that, electrons produced by an electrons gun are injected into the accelerator waveguide
- The accelerator Structure then accelerates the electrons from an electron gun using microwave power from the power source.

- Finally, High-energy electrons emerge from the exit window of the accelerator guide as a pencil beam; these electrons are made to strike the target to produce X-rays or strike the scattering foil to use electrons to treat tumors [9].

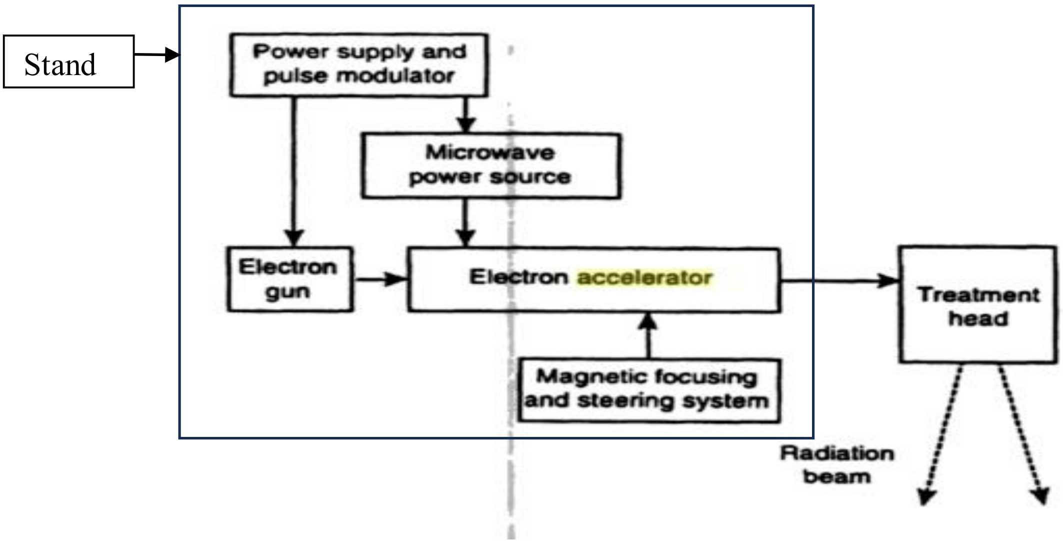

Figure2.2. *Diagram showing the different components of the linear accelerator that are needed for the generation of the radiation beam. These components are located within the stand of the Linac [9].*

2.4.3.Linac's Head

It is essential to describe in detail the CMs of the Linac's head that impact the output beam. The target, the primary collimator, the FF, the ionization chamber, the mirror, and the secondary collimator are examples of these parts that are frequently utilized. The parts of the Linac that have the most impact on the photon spectrum's form are the target, the primary collimator, and the FF [10], [11], [12].

Instead of being accelerated by the potential difference like in orthovoltage and superficial x-rays, electrons in a linac used for RT gain energy by interacting with an electromagnetic field of synchronized radio frequency. The accelerator construction comprises a long, cylindrical tube with several circular deflectors [13]. Magnetic fields bend the electron beam as it exits the accelerator tube, resulting in a collimated beam with a width of about 2 to 3 mm that hits the target normally [14], [15]. An illustration of the components of a typical Linac treatment head in photon beam mode are shown in Figure2.3.

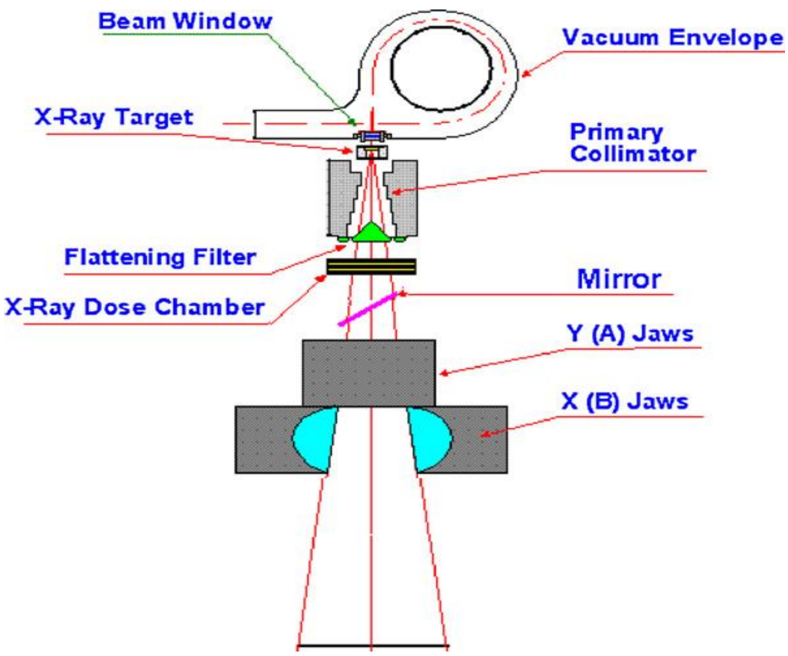

Figure2.3. *Illustration of the components of a typical Linac treatment head in photon beam mode [16].*

Figure2.4 shows the target of the Linac machine. The function of the target in the Linac's head is to convert the electron beam into photons. The material and thickness of the target have a considerable impact on the photon beams generated. Initially, The target material was gold, water, steel, and graphite. Still, later, other materials like tungsten and copper that were thin enough to block the primary electrons were added. Some researchers utilizing the MC approach found that the target material of Tungsten (W), Titanium (Ti), and Tantalum (Ta) is ideal because an efficient photon beam is created. The atomic number (z) for W, Ti, and Ta are 74, 22, and 73, respectively. Using aluminum (Al) and lead (Pb) in the target material to deliver photon-beam treatment has also significantly contributed to RT technology [3]. The z numbers for Al and Pb are 13 and 82, respectively.

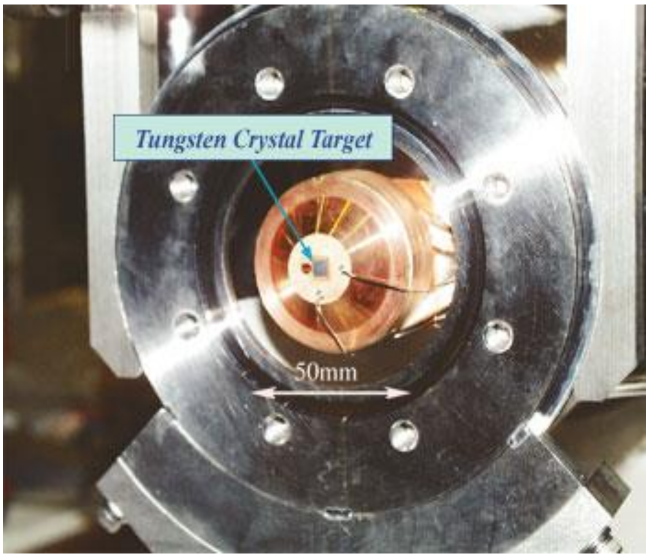

Figure2.4. *Target assembly: The tungsten crystal is fixed to the cylindrical copper body for water cooling.*

The collimators are used to confirm that only the treatment region is exposed to radiation. The linacs possess more than one collimator. The primary collimator is the first set of lead blocks and stationary. They define the maximum x-ray beam size, which is usually 40x40 cm^2. The secondary collimator is two pairs of jaws made from tungsten that move in opposite directions. These two pairs of jaws can close or open to increase or decrease the size of the exposed area. A multileaf collimator (MLC), seen in Figure2.5 is often located below both. Like jaws, the MLC is frequently constructed from tungsten, a known high z material. It usually contains 80 to 120 interdigitating tiny, long, rectangular-shaped leaves that move individually in a single plane [17].

The FF, seen in Figure 2.6, mainly aims to flatten the cross-section of the entering beam profile, which is centrally peaked. This is why the filters are typically circularly symmetric and have a conical form. It is located above the set of collimators. The FF attenuates the soft energy x-ray photons from the spectrum, making the beam harder [17], [18].

Figure2.5. *MLCs showing an aperture. Image courtesy of Varian Medical Systems, Inc. All rights reserved.*

Figure2.6. *FF with a conical shape thick in the center and thin in the periphery to attenuates more photons*

2.5. Flattened and Unflattened Beam

The FF was first designed to generate flat dose profiles at a certain depth. After over 30 years of being a staple of therapy in the medical field, modern linacs systems have eliminated the requirement for an FF. The applicability of the FFF photon beam has been intensively studied recently. Previous research has shown that FFF beams are more advantageous than FF beams; however, it is necessary to ensure accurate measurements and better planning to protect the health of the cells [20], [21], [22], [23], [24], [25].

The characteristics of the FFF beam are as follows:

2.5.1. *Beam profile*

Figure2.7 represents the difference between the beam profile of the FF and FFF beams. The main feature of the FFF beam is its forward peaked dose profile. The center of the FFF beam will have the highest dose, while the field edge will have a steadily decreasing dose. In contrast, the FF in the FF beam is used to flatten the beam profile with a Gaussian shape [26].

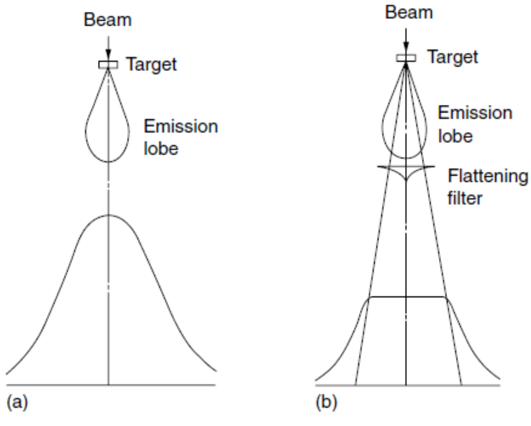

Figure2.7. *Photon beam profile of medical Linac (a) without and (b) with FF [13].*

2.5.2. Dose Rate

The dose rate of the FFF beam is higher than that of the flattened beam, and it is one of the essential effects of removing the FF [21], [23], [24], [25]. The reasons behind increasing the dose rate in the FFF beam over the FF beam is that a significant portion of the primary photons from the center of the beam is removed by the FF in the Flattened beam, especially near the central axis, and more primary photons experience attenuation.

2.5.3. Treatment Duration

Clinical deployment of the FFF beam would decrease treatment duration by increasing the dose rate [27]. Some motion control approaches, like breath-hold and primarily for treating small field sizes (FS), will benefit from shorter delivery times [28].

2.5.4.Surface Dose

Due to the increased incidence of contaminant-charged particles and low-energy photons in FFF beams, the surface dose values of FFF beams were greater than those of FF. [21], [26], [27], [28], [29].

2.5.5.Beam Quality

Beam quality can be described using an energy spectrum curve. The energy spectrum of the beam is considered a good indicator of whether the beam is hard or soft. The presence of the low-energy photons in the photon spectrum of the FFF beam makes the beam soft. Thus, the FF beam is harder than the FFF beam, so it has better beam quality [30].

2.6. MC

2.6.1.MC Method

MC methods are stochastic strategies for problem-solving that rely on using random numbers and probability statistics [31]. MC techniques have been used with different aspects of RT, from modeling radiation treatment devices and sources to dose calculation in different geometries [32]. The basic procedure for modeling radiation transport first needs information regarding the entering particles, such as their kind, position, direction, and energy. After that, the type of interaction (such as Compton scattering, photoelectric effect, etc.) is identified. The new energy and direction of the particle are specified according to the type of interaction, and the transport of any secondary particles generated by this interaction is then modeled in the same method. In the MC simulation for the linac head, the quantity of interest, for example, the energy deposition in every voxel, may be determined using many simulations (histories). For dose calculation, the dose is scored over volume elements (voxels) of small size [33].

However, the MC simulation technique has a significant limitation depending on the long computation time associated with MC simulation, making this technology unfeasible for everyday clinical treatment planning. Calculation times have been considerably reduced using variance reduction techniques, such as defining the energy cut-off for photons and electrons [32],[34].

2.6.2.MC Software

For radiation transport modeling, many general-purpose MC software has been created, such as EGS4 [35],electron gamma shower (EGSnrc) [36], MCNP [37], and GEANT [38]. The MC software used in this research is EGSnrc.

EGSnrc is a set of computer programs called electron–gamma–shower used to model photon and electron transport using the MC technique [36]. This software includes more than one code, and each is used for different features. These codes are BEAMnrc [39], BEAMdp [40], and DOSXYZnrc [41]. Radiation treatment beams are modeled using the MC modeling software BEAMnrc [39], based on the EGSnrc system. After modeling the Linac using BEAMnrc, BEAMDP was used as a general-purpose beam utility software to extrapolate energy, planar fluence, mean energy, angular distributions, etc., from a current phase-space data file produced by BEAMnrc [40]. After that, DOSXYZnrc is an MC modeling system based on EGSnrc that estimates the deposition of the dose [41].

3. Literature Review

Vimolnoch, M. et al. conducted a study evaluating the Varian TrueBeam phsph file supplied by the manufacturer. A 6 MV photon beam energy modeled for small fields. The work was done using the EGSnrc simulation system, and the simulation data was subsequently compared with measurements. The paper illustrates that the findings from the MC simulation agree with the measurement for 1x1 cm^2 FS and larger. These results demonstrate the feasibility of using the 6 MV Varian phsph file as a radiation source for precise MC dose estimation in a small field [42].

Ghemiş, D. M., & Marcu, L. G. performed a study reviewing the state of knowledge on FFF beams and their use in SRS and stereotactic body RT (SBRT) while focusing on two of the FFF beam advantages treatment duration and sparing organs at risk. A PubMed search was conducted using key phrases to find related papers. The study shows that sharp dose fall-off is related to increased OAR sparing in FFF beams. Moreover, treatment plans delivered with FFF plans had a similar or better dosimetric outcome than those supplied with FF beams [43]. Vassiliev, O. N., et al. executed a study on how FFF beams can replace traditional FF beams in SBRT treatment plans for lung cancer. A sample of patients who had encountered SBRT with 6 MV FF beam earlier are involved in the study. The treatment plans were imported into the system and modified to a new plan with an FFF beam instead of the conventional 6 MV photon beams. The study shows that FFF beams could provide lower doses to organs at risk while preserving tumor coverage. Therefore, switching FF beams out for FFF beams can improve the therapeutic ratio [44].

Pokhrel, D. et al. performed a study to quantify the differences in dosimetry as a function of ipsilateral lung density and treatment delivery parameters for stereotactic, single dose of volumetric modulated arc therapy (VMAT) lung stereotactic body radiation therapy (SBRT) delivered with 6 MV FFF beams compared to 6 MVFF beams. The study was affected by 13 consecutive early-stage I–II non-small-cell lung cancer patients. Those patients were treated with highly conformal noncoplanar VMAT SBRT plans using 6 MV-FFF. After that, treatment plans were reoptimized with 6 MV FF beams for identical beam/arc geometries and planning objectives. The findings of this study were that 6MV FFF VMAT plans for stereotactic single-dose lung SBRT provided similar target coverage with better dose conformity, improved OAR sparing compared to traditional 6 MV FF beams, and significantly reduced treatment time [45].

Zeghari A. et al. conducted a study examining the impact of the FFF beam on improving the surface dose and dose at the buildup region. This study was designed using the EGSnrc package, an MC simulation system. The energy of the beam used was 12 MV. The paper shows that using an unflattened photon beam will significantly increase the surface dose and dose at the buildup region, which may be beneficial for treating various skin malignancies [46].

Mohammed, M. et al. executed a study comparing and evaluating the dosimetric characteristics of 6 MV FF and FFF photon beams. This work was done by using a simulation technique. EGSnrc (BEAMnrc and DOSXYZnrc user's codes) is the simulation system used. The paper shows a variation in the dosimetrist characteristic between the FFF and FF beams. Moreover, FFF can effectively target cancer cells while preserving the surrounding healthy tissue [26].

Shende, R. et al. perform a study to compare and analyze beam data measured with FF and FFF beams in quantitative and qualitative terms using a Varian TrueBeam Medical linac and IBA dosimetry system in a water phantom. The study result was differences in various parameters, for example, percentage depth dose (PDD) curves, Surface dose, symmetry, --etc [30].

Sigamani, A. et al. conducted a study using a Varian TrueBeam linac to assess the central axis dose in the buildup region and the surface dose of a 6 MV and 10 MV FF and FFF photon beam for various FSs. A parallel plate ionization chamber measures the surface dose in a solid water phantom. The FFF beams for both energies have a slightly larger surface dose in the buildup region than FF beams. Regardless of the detector and photon beams' FF or not, the surface dose rises with increasing FS [47].

LU, Jiayang, et al. performed a study evaluating the dosimetric impacts of FFF beams in IMRT and VMAT for sinonasal cancer. The study was conducted using fourteen cases, and IMRT and VMAT planning was performed using 6MV photon beams with FF and FFF beams. The study showed that FFF beams led to comparable target dose homogeneity, conformity, increased number of MUs, and lower doses to the spinal cord, brainstem, and normal tissue, compared with FF beams in both IMRT and VMAT [48].

Belosi, M. F., et al. compared the accuracy of the FFF beams distributed phsph files to actual measurements. The work was done using the PRIMO simulation system. The study found that MC simulations are compatible with experimental data, especially for fields up to 10x10 cm^2. Regarding this agreement, TrueBeam's Varian phsph files for FFF beams can be used as radiation sources for precise MC dose calculation [49].

Javedan, K. et al. investigated the superficial dose from FFF beams compared to the FF. EGSnrc MC simulation system is used in this study. The findings of this study showed that due to the lower mean energy in the FFF beam, the clinical superficial dose is higher in the FFF beams compared to the FF beam [50].

Jaafar Sidek, M. conducted a study to gain more information on the FFF beam of the 6 MV Elekta linear accelerator. This study was done using MC simulations. The results of the study are validated by comparing them with measurement data. MC findings of the study show excellent clinical characteristics for FFF beams in which there is reduced total scatter and lower leakage radiation [51].

4. METHODOLOGY AND SIMULATION SETUP

4.1. Simulation and Analysis Software

EGSnrc is a MC simulation software designed to simulate radiation transport by simulating the interaction of particles, electrons, photons, and positrons with matter. The EGSnrc software is the simulation engine and comes as a package that includes three codes used to reach the required results BEAMnrc, BEAMdp, and DOSXYZnrc. These three codes are detailed in sections 3.3, 3.4, and 3.5. We chose BEAMnrc to build the linac because it has readymade components that can be modified and adjusted easily. Moreover, DOSXYZnrc simulates the dose distribution by simplifying the choice of the phantom material and geometry. Also, BEAMdp can quickly analyze the phsph files.

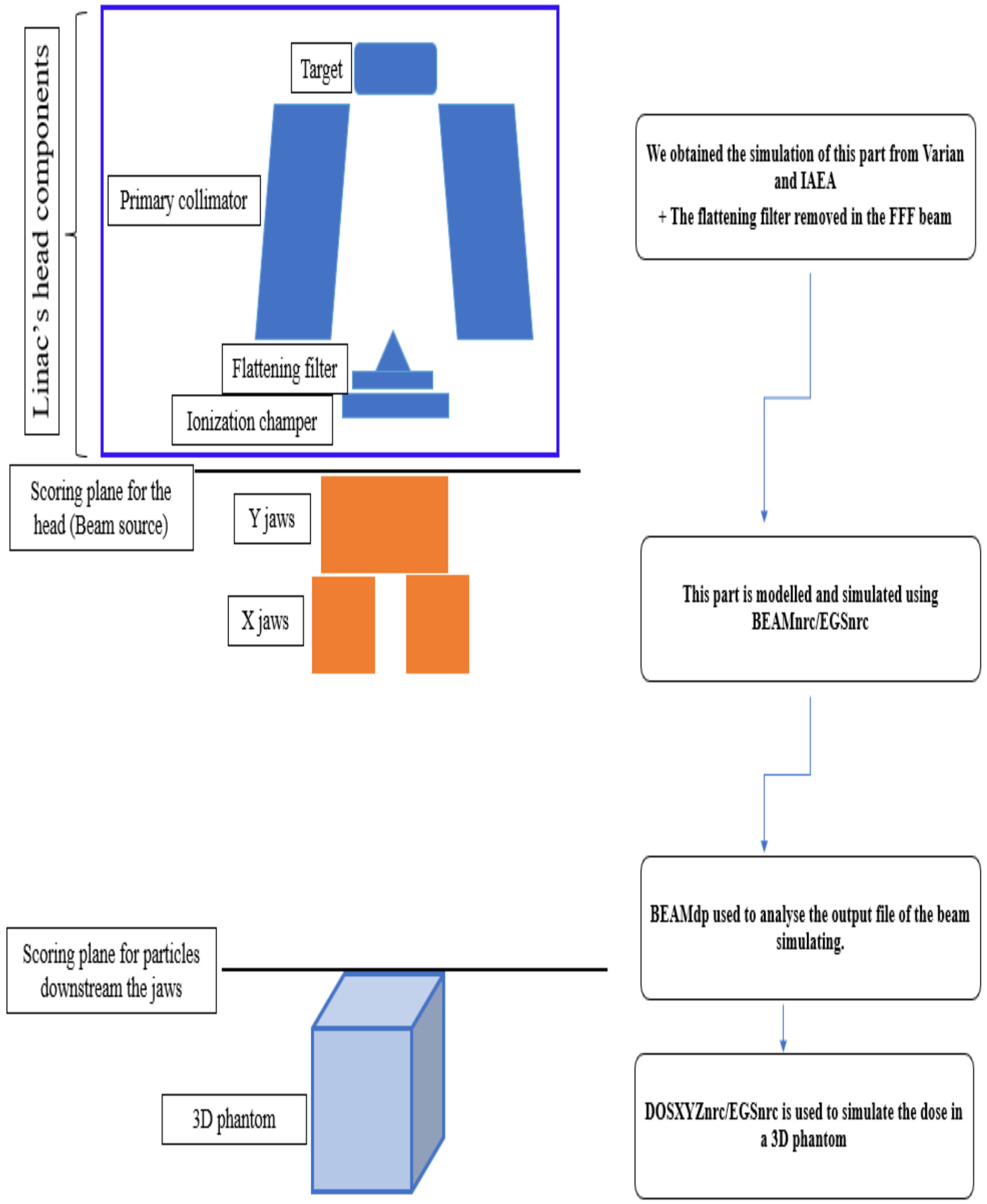

Figure3.1. *A representation illustrating the sequential steps of the simulations.*

4.2. Linac Modeling and Simulation

Modeling and simulation of any Linac require details of the components used for Linac constructions in terms of the material and dimensions used. These details are usually confidential to the manufacturer company for commercial reasons. However, Varian provides the clients and researchers with phsph files to simulate the Linac head (from the target to just above the jaws). These simulations were scored at 27.88 cm from the target and stored in a phsph file. This study used these phsph files as a beam source in the BEAMnrc. The MC model of the Linac from the jaws and below was built based on the manufacturer (Varian et al., USA).

4.2.1.The FFF beam linac model and simulation

This section describes the construction of the Linac model of the FFF beam used in this study. Figure 3.2 shows the linac construction from the scoring level of the Varina 27.88 cm and below. The passage of the beam was simulated and scored at source-to-surface distance (SSD)=100 cm. The CMs listed below were used to construct the Linac downstream of the jaws.

1. CM1 slab: A vacuum slab has a thickness of 0.01 cm and is located at 27.88 cm from the reference plane, directly above the movable jaws, as illustrated in Figure 3.2. Varian phsph file, which simulates the particles' transport in the head, was stored on this CM and used as a beam source.
2. CM2 Jaws: Linac has two pairs of tungsten jaws above each other. These jaws are moveable and used to define the FS. The upper pair of jaws move along the y direction, while the lower jaws move along the x direction. The x and y jaws are 36.66 cm and 27.89 cm from the reference plane. The described configuration is graphically shown in Figure 3.2. Simulations are carried out for FS ranging from 6x6 cm^2 to 40x40 cm^2.
3. CM3 slab: A water slab with a thickness of 0.01 cm is added at 100 cm SSD, which can be seen in Figure 3.2. This slab was only for scoring the particles at this level; all the particles reaching the end of the water slab were stored in another phsph file. We used the phsph file scored at this level as a beam source for dose simulation in a water phantom.

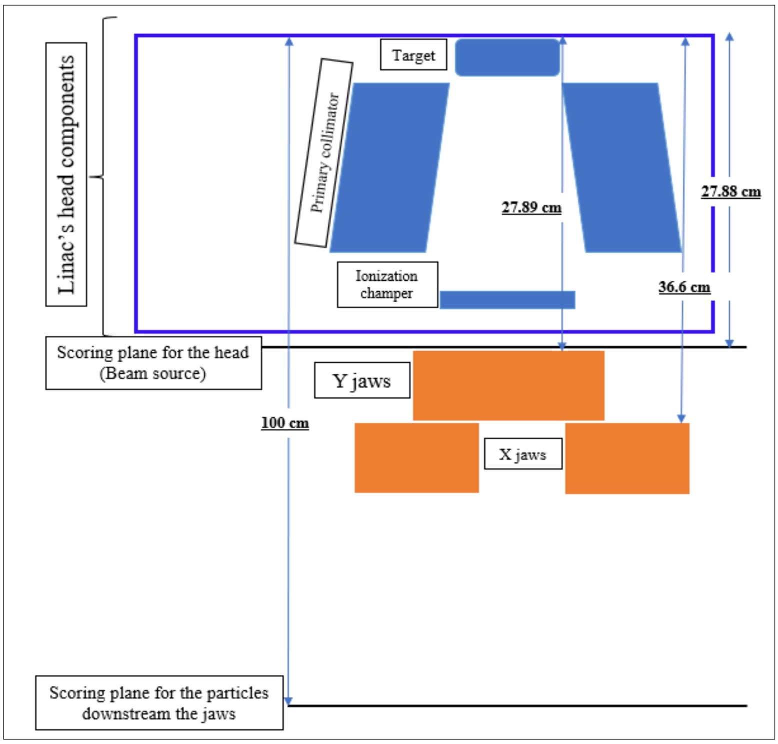

Figure3.2. *Linac model constructed by BEAMnrc user code for simulating the FFF beam. This model is charictarized by the elimination of the FF from the path of the beam.*

Figure 3.3 shows the graphical interface for BEAMnrc and other associated windows. The number of histories for the FFF beam was $2x10^7$ histories, which is the same as the number of particles in the phsph file. The variance reduction techniques are applied to reduce the time and uncertainties. The photon and electron cut-off energies adjusted at 10 keV (PCUT) and 711 keV (ECUT), and the rejection of the electron range was 1 MeV (ESAVE).

4.2.2.The FF beam Linac Modeling and Simulation

This section describes the construction model of the FF beam. Figure 3.4 shows the Linac simulation model for this beam configuration. The phsph file for the FF beam was obtained from Intrnatioal

Atomic Energy Agency (IAEA) [52]. Furthermore, because the number of particles in the phsph varied, the number of histories for the FF beam was $5x10^7$. Similarly to the FFF beam, we simulate the linac from the jaws and below.

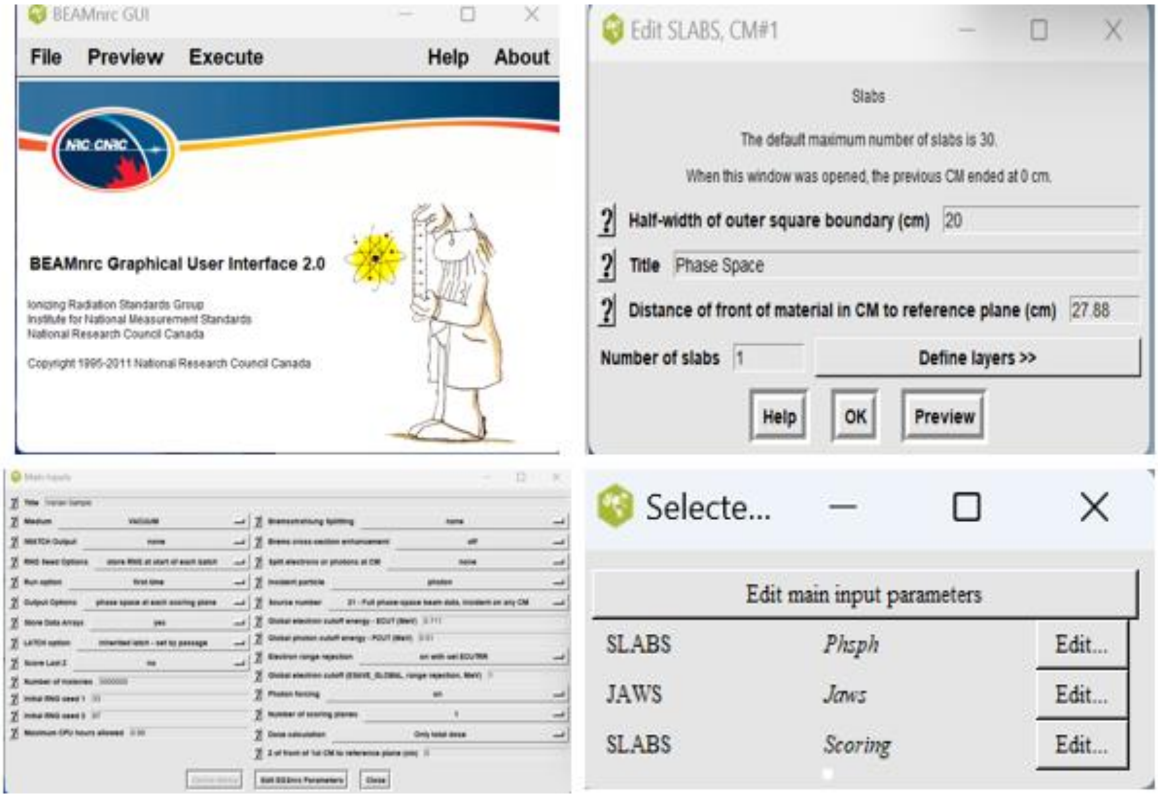

Figure3.3. *Upright: the graphical interface of BEAMnrc user code. Uplift: CM setup window. Downright main BEAMnrc inputs window. Downleft: The modeled components window of BEAMnrc.*

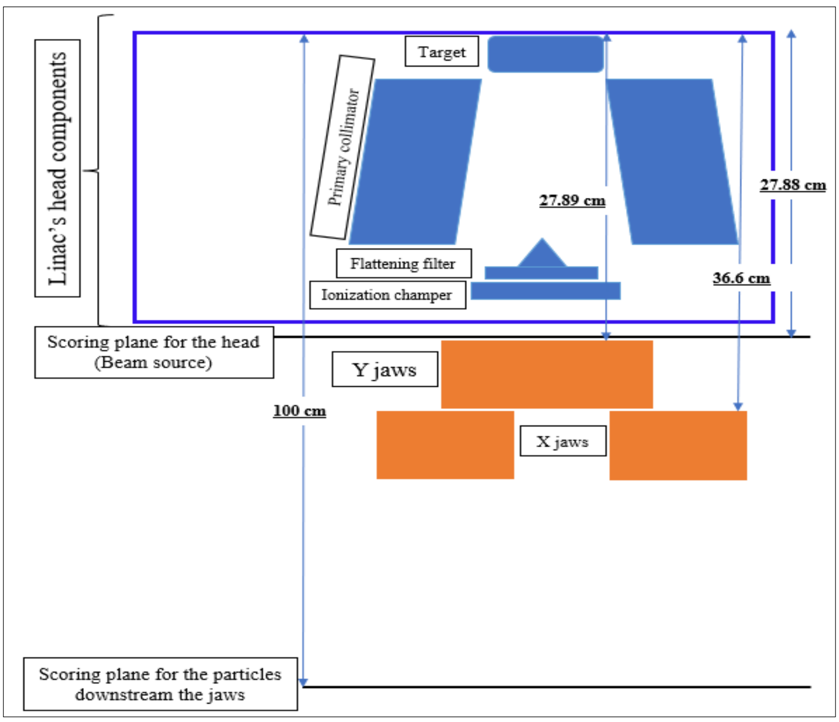

Figure3.4. *Linac model constructed by BEAMnrc user code for simulating the FF beam.This model is charictarized by the presence of the FF in the path of the beam.*

4.2.3.The FFF Beam With Low-Z Material Filters Modeling and Simulation

In this part of the study, we added filters from low-z material to the FFF beam. Figure 3.5 represents the Linac model for simulating the FFF beam with a low-z material filter. We add the filters with different thicknesses between the jaws and the scoring plane at 44.45 cm from the reference plane. These filters are from Al and steel, which have an atomic number of 13 and 26, respectively. All other settings are similar to the FFF beam model.

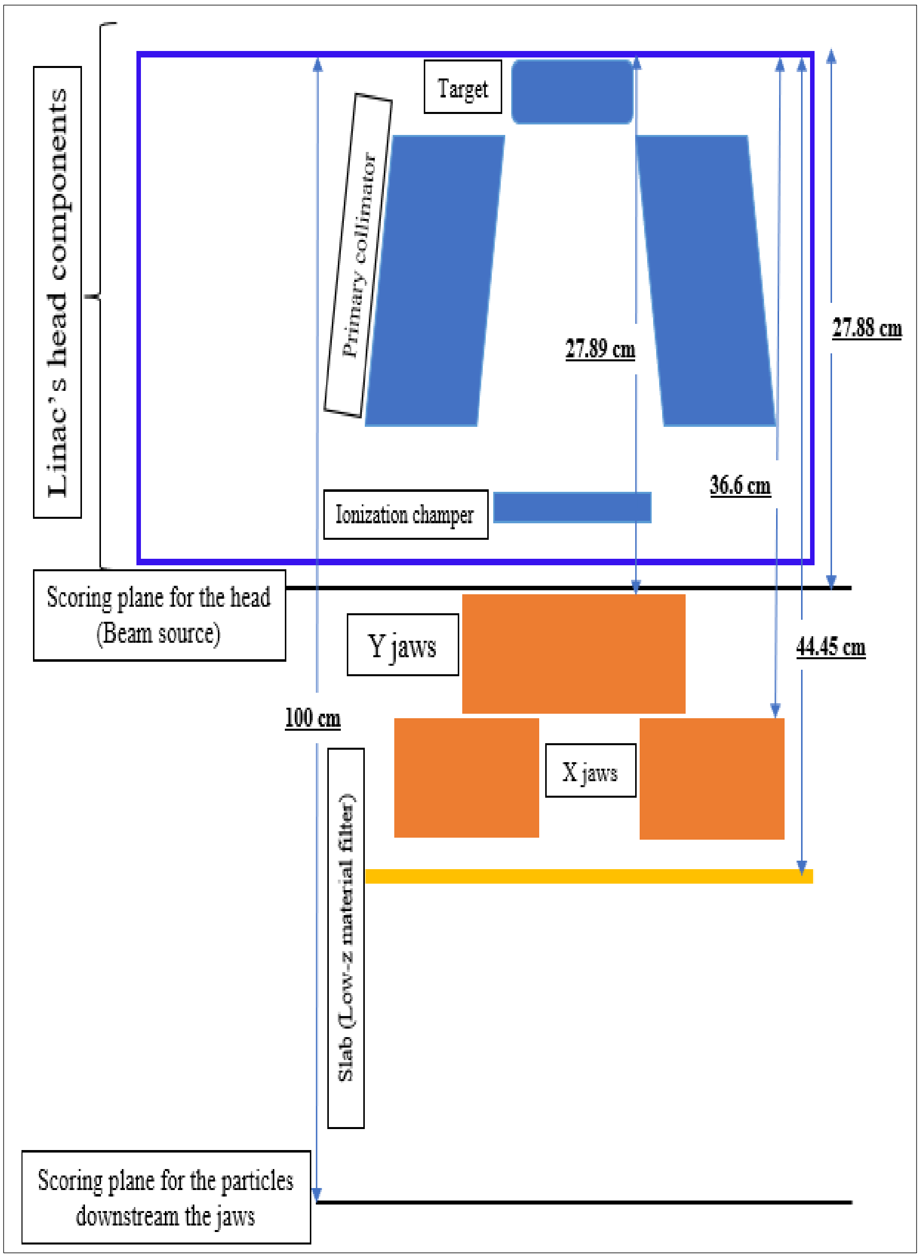

Figure3.5. *Linac model constructed by BEAMnrc user code for simulating the FFF beam with low-z material filter. This model is charictarized by the y the elimination of the FF from the path of the beam and adding low-z filter below the jaws.*

4.3. Phsph File Analysis

To analyze the phsph files, we used the BEAMdp user code. First, the energy spectrum of the beam was analyzed from the egs phsph file. The energy fluence distribution main inputs window is shown in Figure 3.6. All the particles with energies up to 6 MeV in the phsph file were analyzed according to the primary incoming photon beam. Also, the particles were analyzed in a rectangular field with rectangular regions of equal area; the dimensions of the rectangular field were set according to the FS. Moreover, the number of bins is set to 200, the maximum allowed number to get a higher energy bin for the spectrum. To compare the beam quality of different configurations, we normalize the planar energy fluence to unity as follows:

$$\frac{\text{Planar energy fluence}}{\text{Maximum planar energy fluence}} \text{x100}$$

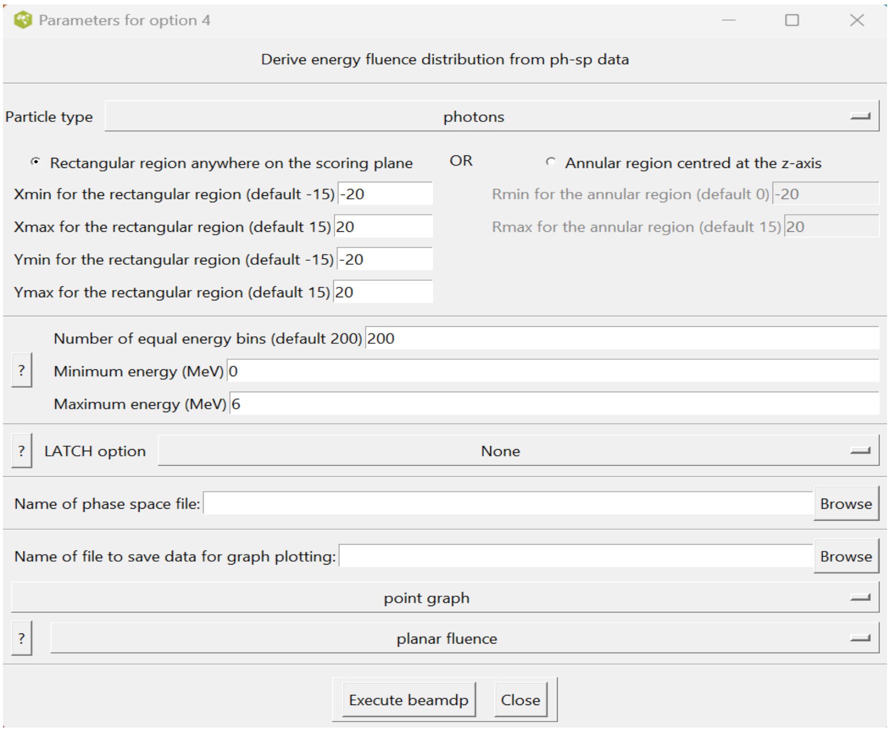

Figure3.6. *The main inputs window for extracting and analyzing the energy fluence distribution from the phsph file.*

4.4. Dose Simulations

The graphical interface of DOSXYZnrc and the inputs window is shown in Figure 3.7. DOSXYZnrc/EGSnrc was used in the interface to simulate the dose distribution. The phsph file resulting from simulating the beam was used as the beam source for the simulations in DOSXYZnrc. We simulated the dose distribution in a homogeneous water phantom at a distance of 100 cm from the target. The phantom and voxel dimensions are shown in Figure 3.8. The lateral dimensions of the phantom (x, y) were defined to be slightly larger than the FS at the surface by a margin of 2 cm, as illustrated in Table 3.1. The depth of the phantom (z) was 64 cm for all the FSs.The phantom was divided into many small voxels. The voxel dimensions are 1x1x0.5 cm^3 for the FS from 6x6 cm^2 to 20x20 cm^2. These dimensions are selected to obtain a better result with less noise. The number of histories is set to be $8x10^8$, and no variance reduction techniques are used.

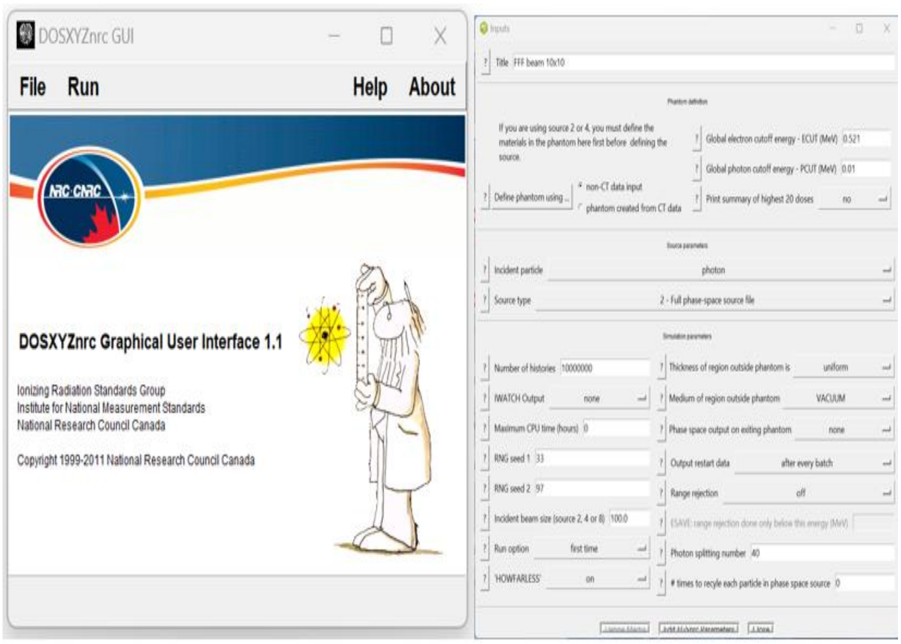

Figure3.7. *Left: the graphical interface window of DOSXYZnrc user code. Right: DOSXYZnrc main inputs window*

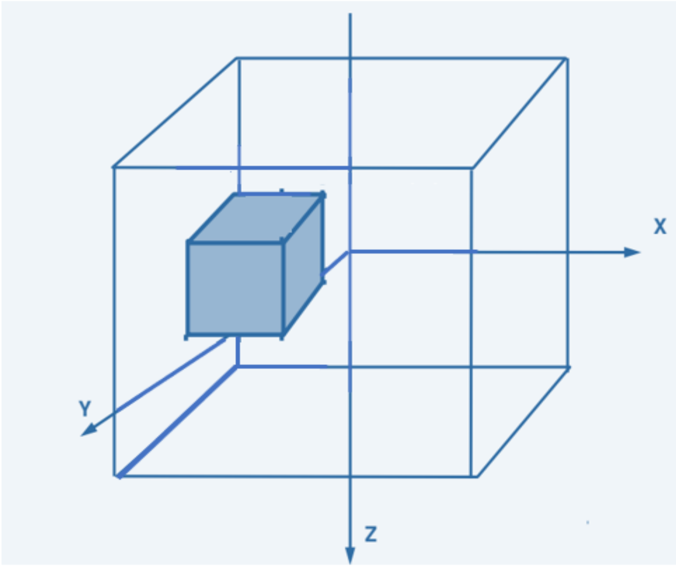

Figure3.8. *Water phantom is divided into small voxels; each voxel has the dimensions 1x1x0.5 cm^3.*

Table3.1. *Dimensions of the phantom with respect to the field size.*

FS (cm^2)	Phantom dimension (cm^3)/ (x, y, z)	Voxel dimension (cm^3)/ (x, y, z)
6x6	8x8x64	1x1x0.5
10x10	12x12x64	1x1x0.5
15x15	17x17x64	1x1x0.5
20x20	22x22x64	1x1x0.5
40x40	42x42x64	1x1x0.5

4.5. Analyzing 3D dose files

The output of the DOSXYZnrc simulation is in the form of 3ddose and was visualized and analyzed using MATLAB [53] and EXCEL. Moreover, the dose profile was evaluated according to the surface dose and the PDD. The PDD curves for all beam configurations were normalized to the maximum dose (d_{max}) to study the surface dose using the following formula:

$$PDD = \frac{\text{Dose at depth}}{\text{Dose at Dmax}} x100$$

4.6. Conclusion

In summary, the steps of the current study are outlined below. The construction and simulation of a Linac downstream the jaws of a 6 MV photon beam of a Varian TrueBeam medical accelerator were performed using the BEAMnrc/EGSnrc MC technique. The linac head geometry from the target to just above the jaws is confidential to the manufacturer, so the manufacturer provides the user with a phsph of the particle's transport in this area (Varian et al., USA). The energy spectra of the FF, the FFF, and the FFF with low-z filter beams were obtained by analyzing the phsph files with the BEAMdp/EGSnrc software. The simulations of dose distribution were obtained using DOSXYZnrc/EGSnrc in a three-dimensional (3D) homogeneous water phantom, with measurements taken at a source-to-surface distance (SSD) of 100 cm.

5. Results and Discussions

5.1. Validation of phsph data

The phsph files for 6MV FF and FFF beams were acquired from the IAEA and Varian Medical system [54], [55], respectively. These files were scored on a plane just above the movable jaws; as discussed in detail in 3.2, the construction of the linacs above the jaws is confidential to the manufacturer. Nevertheless, when employing the phsph provided by Varian and IAEA, users must only encode the geometric details of the True-Beam linac downstream of that plane into their MC simulations setup. These phsph files provide detailed information about each scored particle's type, energy, and position. Also, the files are validated by independent researchers by comparing the results of the MC simulations with experimental data [56], [57].

5.2. Energy spectrum

5.2.1.Beam Quality

Beam quality is a term used to describe the energy spectrum of the beam. Moreover, it determines the penetration range of the beam. The two words soft and hard are used to describe the quality of the beam. A hard beam means more high-energy photons in the spectrum, while a soft beam means more low-energy photons.

5.2.2.The FFF Beam Quality

Figure 4.1 shows the photon energy spectra of a 6 MV photon beam for both FFF and FF beams. In this simulation setup, no jaws are used, so we have an open field 40x40 cm^2 measurement. This figure will be discussed later in the fluence rate. These curves were normalized to the maximum fluence, as shown in Figure 4.2, to investigate the effect of removing the FF on the beam quality. The spectrum consists of a continuous part representing the bremsstrahlung X-ray and a sharp peak representing the characteristic X-ray. The curves clarify that the absence of the FF will shift the energy peak of the maximum fluence of the bremsstrahlung x-ray to a lower energy value. The bremsstrahlung peak energy for the FFF and FF beams was found to be 0.555 MeV and 0.855 MeV, respectively. Table 4.1 represents a numerical value for the photon fluence after normalizing the curves at some energy points for both beam configurations. The photon fluence of the FF beam is seen to be greater at energy levels of 1 MeV and beyond, whereas the FFF beam exhibits a higher photon fluence at energies below 1 MeV. The absence of the FF from the beam's path will increase the low-energy photons, so the FFF beam becomes softer than the FF beam. The FF is made mainly from tungsten, a high-z material. Tungsten attenuates more low-energy photons from the beam than the high-energy ones, so the hardening effect appears in the FF beam.

The change in the beam quality when removing the FF from the beam's path was reported in the related studies. Mohammed et al. studied the FFF beam quality and dose characteristics for Varian 2100 linac using MC simulation and experimental measurements in different field sizes. They reported that the FFF beam is softer than the FF beam and correlated it with higher energy deposition in the buildup region. Moreover, an experimental study by Shende et al. used 6 MV and 10 MV for the Varian true beam and found that the beam quality of the FFF is less than that of the FF beam by 5.4% and 4.5% for 6 MV and 10 MV, respectively [26], [30].

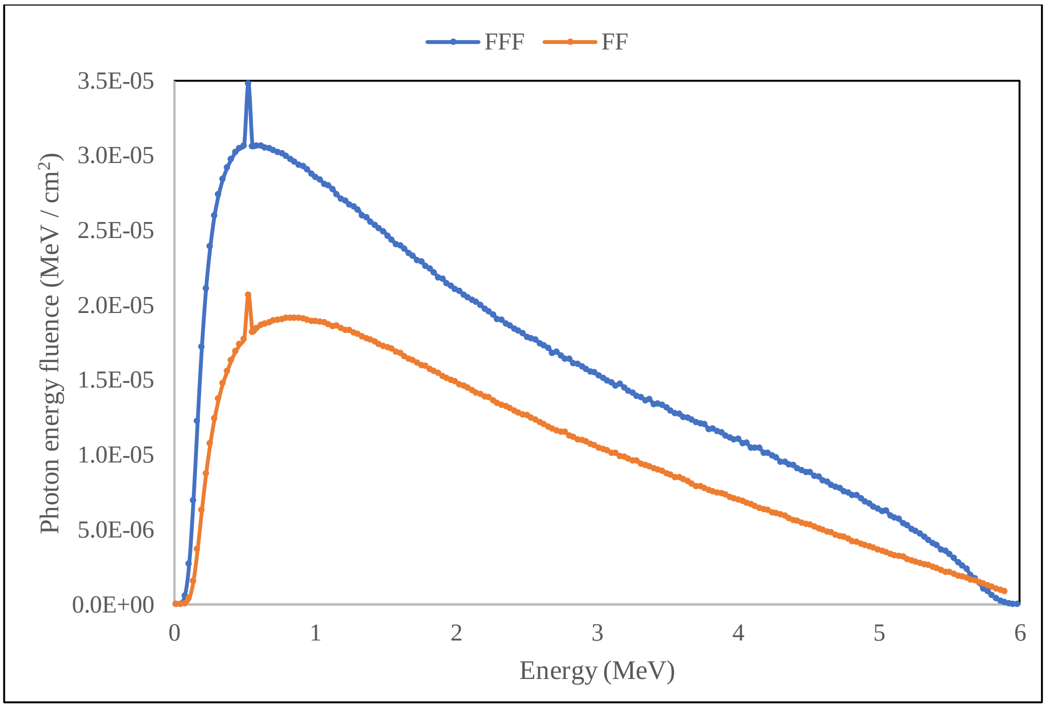

Figure4.1. *Photon energy spectra of the FFF and FF beams for the open field (40x40 cm^2).*

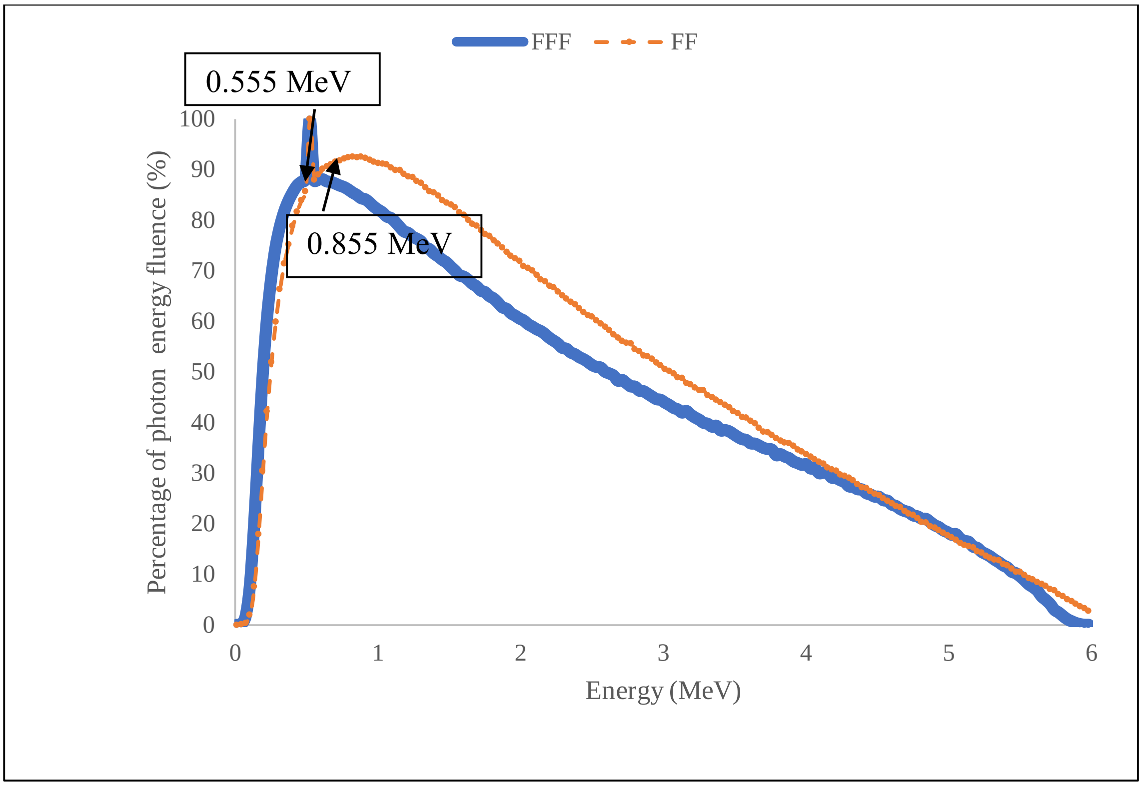

Figure4.2. *Normalized photon energy spectra of the FFF and FF beams for the open field (40x40 cm^2).*

Moreover, we study the energy spectra at different filed sizes, precisely square FSs with widths of 6x6, 10x10, 15x15, and 20x20 cm^2 for FF and FFF beams. FSs are adjusted by the distance between the jaws, as explained in detail in 3.2.1. Figure 4.3 and Figure4.4 represents the energy spectra of the FFF and FF beams with different FSs after normalization. An inset from Figure 4.3, which clarifies the difference between the curves, is presented in the corner of the figure. The figures show that the beam becomes softer as the FS increases for both configurations. Moreover, the effect of change in FS is more apparent in the quality of the FF beam. The distribution of the photons in the bremsstrahlung X-ray may explain this variation. High-energy photons exit the target with small angles and are distributed in the center. In contrast, the low-energy photons exit from the target with large angles and are distributed near the boundaries of the beam.

Some studies (Mesbahi, Mohammed, et al.) discussed the effect of the field size on the energy spectrum. Mesbahi studied A 6 MV photon beam of a Varian Clinac 21EX linac with MC simulations and found that the mean energies of spectra were higher for smaller field sizes. In a study conducted by Mohammed et al., employing MC simulations, a 12 MV photon beam was utilized to investigate the relationship between field size and the mean energy of spectra. Their study found a decrease in the mean energy of spectra as the field size increased. The increase in field size allows for a higher number of low-energy photons to be absorbed by the block and contribute to the spectrum of the beam, resulting in a decrease in average energy [58], [59].

Table4.1. *Photon energy fluence for the FFF and FF beams at selected energy is taken from Figure 4.1.*

Energy (MeV)	FFF Beam (% photon fluence)	FF Beam (% photon fluence)
0.25	68.7	52
0.5	88.1	85.7
1	82.1	91.3
2	60.6	71.9
3	44.5	51.3
4	31.7	33.8
5	18.3	17.7
6	12.7	27.7

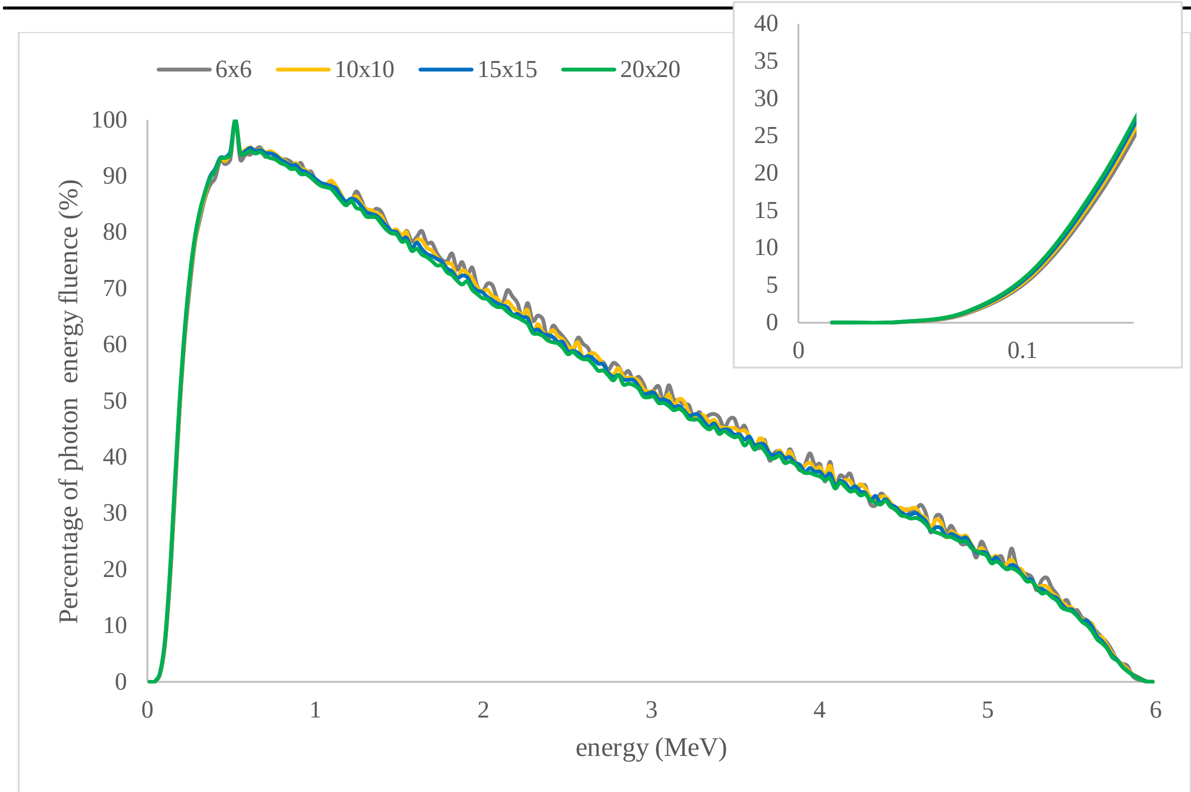

Figure4.3. *The FFF beam's energy spectrum of different FSs ranges from 6x6 to 20x20 cm^2. The inset is a zoom region from 0 to 0.1MeV to clarify the difference between the curves*.

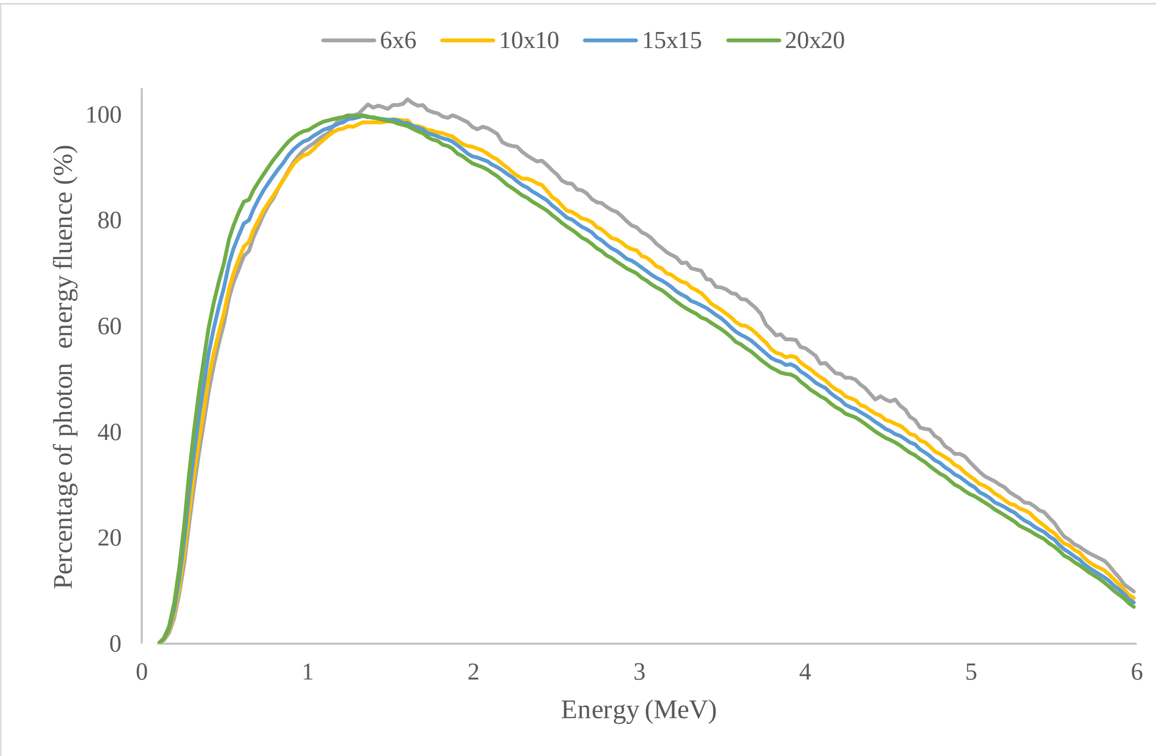

Figure4.4. *The FF beam's energy spectrum of different FSs ranges from 6x6 to 20x20 cm^2.*

5.2.3.Quality of the FFF beam with low-z material filters

The filters chosen for the study were steel and Al. Figure 4.5 shows the mass attenuation coefficient (μ) curves for Al, steel, and tungsten, while Table 4.2 represents the numerical values of the μ for these materials. Figure 4.5 shows that steel has a higher μ than tungsten at low energy, at 10 KeV. With increasing energy, the μ of the three materials decreases. However, the dependence of the μ on the energy differs from material to material. Al has a higher μ than steel in the energy range from

$2x10^{-3}$ to $8x10^{-3}$ MeV. At the same time, the µ of steel has a sharp increase at $8x10^{-3}$ MeV. Beyond 0.01 MeV, the µ of steel and Al drops at a higher rate than tungsten. So, there is a bigger variation in mass attenuation coefficients between tungsten and the low-z materials for energies over 10 KeV.

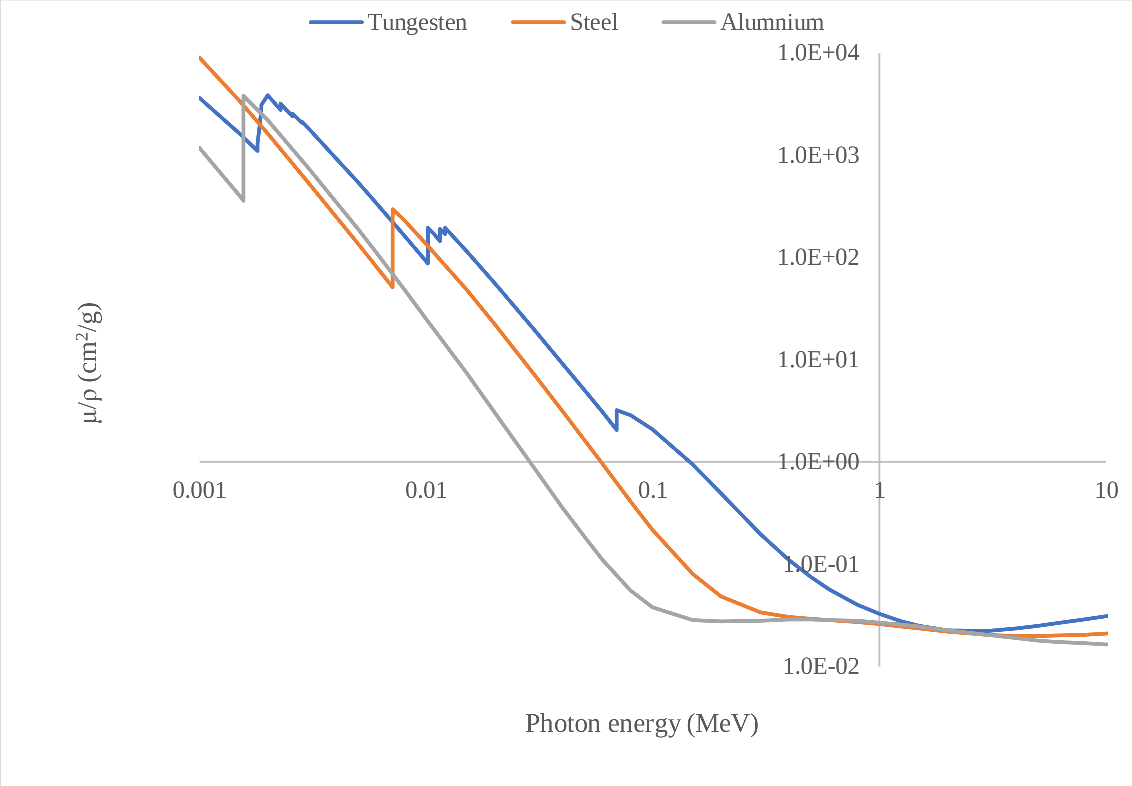

Figure4.5. *The mass attenuation coefficient as a function of photon energy for Al, steel, and tungsten.*

Table4.2. *The mass attenuation coefficient as a function of photon energy for Al, steel, and tungsten.*

Energy (MeV)	μ/ρ (cm^2/g)		
	Al^{13}	$Steel^{26}$	W^{74}
0.008	$4.918x10^{1}$	$2.32x10^{2}$	$1.64x10^{2}$
0.5	$2.87\ x10^{-2}$	$2.91\ x10^{-2}$	$7.44\ x10^{-2}$
0.6	$2.685\ x10^{-2}$	$2.84\ x10^{-2}$	$5.67\ x10^{-2}$
4	$1.88\ x10^{-2}$	$1.990\ x10^{-2}$	$2.36\ x10^{-2}$
5	$1.80\ x10^{-2}$	$1.983\ x10^{-2}$	$2.51\ x10^{-2}$
6	$1.74\ x10^{-2}$	$1.997\ x10^{-2}$	$2.65\ x10^{-2}$

The photon energy spectra in Figures 4.6 and 4.7 show the photon energy fluence of FF, FFF, and FFF with different low-z material thicknesses for steel and Al, respectively. We chose the thickness of the low-z material filter to be 1 cm for a better therapeutic outcome than the FF beam. These figures reflect the fluence rate and will be discussed later. Figure 4.8 and Figure 4.9 show the photon energy spectra after normalization to study the effect of adding steel and Al filters on the beam quality. The use of low-z material filters improves beam quality by causing a decrease in the quantity of low-energy photons within the beam, as these photons are attenuated by the filters constructed from low-z materials. These filters are characterized by attenuating low-energy photons more than the high-energy ones. The bremsstrahlung peak energy for the FFF beam with an Al filter and the FFF beam with a steel filter with different thicknesses is listed in Table 4.3. It can be concluded from these results that using a steel filter improves beam quality more than an aluminum filter. This also shows that the steel filter can absorb low-energy photons more than the aluminum filter.

Table4.3. *The bremsstrahlung peak energy values for the FFF and FFF beam with low-z material filters.*

	Energy peak value FFF with Al filter (MeV)	Energy peak value FFF with steel filter (MeV)
FFF beam +1cm thick filter	0.735	1.10
FFF beam +1.5cm thick filter	0.765	1.25
FFF beam +2.5cm thick filter	1.10	1.64

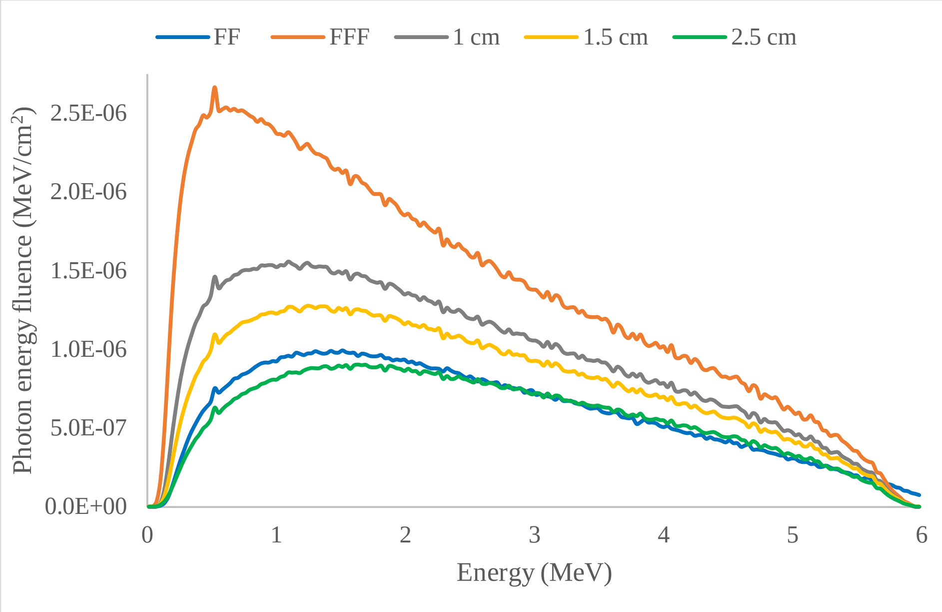

Figure4.6. *Photon energy spectra of FF beam, FFF beam, and FFF beam with steel filter of different thicknesses.*

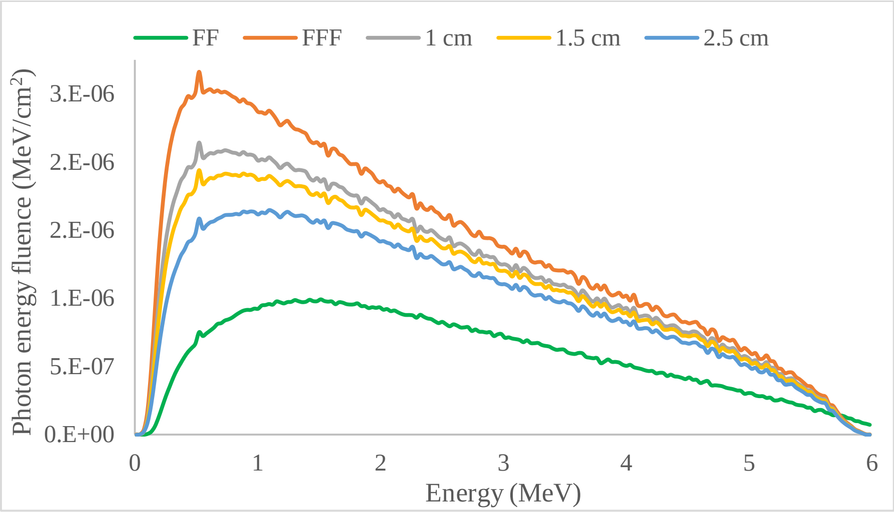

Figure4.7. *Photon energy spectra of FF beam, FFF beam, and FFF beam with Al filter of different thicknesses.*

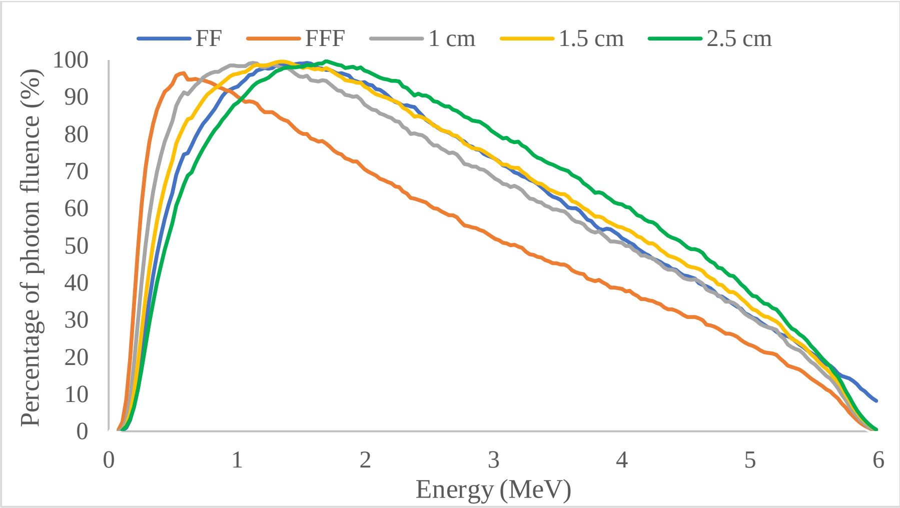

Figure4.8. *Normalized photon energy spectra of FF beam, FFF beam, and FFF beam with steel filter of different thicknesses.*

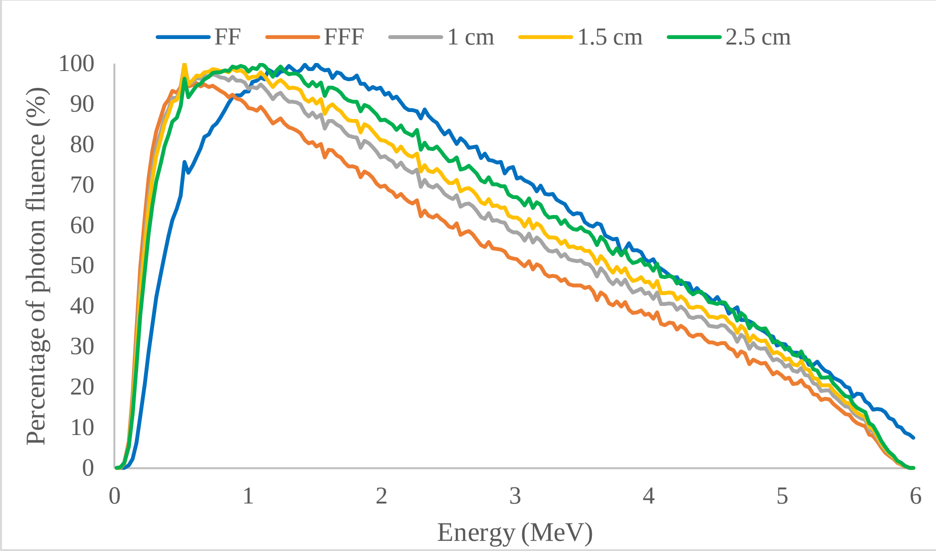

Figure4.9. *Normalized photon energy spectra of FF beam, FFF beam, and FFF beam with Al filter of different thicknesses.*

5.3. Particle Energy Fluence

This section will discuss the photon energy fluence for the FFF, FF, and FFF beams with steel and Al filters. The particle is defined as the amount of energy passing per unit area in a unit of MeV/cm^2. This is an essential discussion in MC simulation because it reflects the dose rate in treatment, which is essential in modern RT.

5.3.1. The FFF Beam Particle Energy Fluence

Figure 4.1 shows the FF and FFF beams' photon fluence spectra for the open field (40x40 cm^2). The numerical values for the maximum photon energy fluence and the percentage of the reduction in the photon energy fluence for all beam configurations compared to the FFF beam are presented in Table 4.4. The maximum photon energy fluence values for the beams were taken from Figure 4.1, Figure 4.6, and Figure 4.7. Based on the data presented in the table, it can be observed that the photon energy fluence of the FF beam was reduced by approximately 63%. According to Figure 4.1, it can be observed that the overall spectrum of the FFF beam exceeds that of the FF beams as a result of the attenuation loss caused by the FF. The photon energy fluence is elevated due to the large number of low-energy photons within the FFF beam, leading to an increased dose given to the patient and a reduction in treatment duration. One benefit of reducing the duration of treatment is that it makes patients more comfortable. It also makes it less likely that the patient's moves will affect how well the treatment works.

The higher dose rate for the FFF beam was reported widely in the literature. A MC study by Mohammed et al. used a 6MV photon beam and found that the FFF beam has a 2.46 times higher dose rate than the FF beam [26]. Another study by Assalmi, M., & Diaf, E. Y., an MC study validated experimentally using a 6MV photon beam and simulated Elekta Synergy linac with different MC codes in two other heterogeneous phantoms and found that the dose rate is higher in the FFF beam by a factor around 2.5 [60]. Shende et al. studied a 6MV and 10MV photon beam experimentally and found that the absence of the FF will shorten the beam delivery time because of the higher dose rates [30]. Moreover, a clinical study by Jaruthien, Thitiporn, et al. confirmed the clinical efficacy and safety of lung SBRT using an FFF beam. This study shows that the FFF technique permits a considerable increase in the dose rate delivery and reduces treatment time by more than 50% compared to the FF beam [61].

Table4.4. *The maximum photon energy fluence and the percentage of the reduction in the photon energy fluence compared to the FFF beam. The Low-z filters had a thickness of 1cm.*

	Maximum fluence (MeV/cm^2)	Percentage of reduction in energy fluence (%)
FFF beam	2.66×10^{-6}	NA

FF beam	9.93 x 10^{-7}	63 %
FFF beam + Al filter	2.14x10^{-6}	19.5 %
FFF beam+ steel filter	1.56 x 10^{-6}	41.4 %

5.3.2.The particle energy fluence of the FFF beam with low-z material filters

Figures 4.6 and 4.7 show the photon energy spectra for the FFF, FF, and FFF beams with steel and Al filters with different thicknesses, respectively. We used different thicknesses of Al and steel to improve the therapeutic outcomes of the FFF beam. Figures indicate that the increase in the filter thickness leads to a decrease in photon energy fluence. Additionally, using filters made from steel thicker than 1.5 cm will make using the FFF beam lose its advantage of the high dose rate. The use of Al and steel filters with the FFF beam resulted in a reduction in the photon energy fluence. The percentage of reduction in the photon energy fluence is 19.5% and 41.4% when adding Al and steel filters, respectively, into the beam's path. However, the dose rate in this instance remains higher than that of the FF beam. It can be observed that the steel material exhibits a greater reduction in dose rate compared to the Al filter. This can be attributed to steel's higher attenuation coefficient than Al, particularly at lower energy levels.

5.4. Dose at Water Phantom

Dose distribution data are measured in a water phantom because it closely approximates the radiation absorption and scattering properties of muscles and other soft tissues. The absorbed dose in the patient varies with many factors, such as distance, FS, beam energy, etc. A 3D dose distribution in a homogeneous water phantom of the FF and FFF beams is shown in Figures 4.10 and 4.11, respectively. The figures illustrate that the FFF beam exhibits a conical profile and that the highest dose is observed at the beam's CA. Conversely, the FF beam shows a uniform dose distribution due to the presence of the FF.

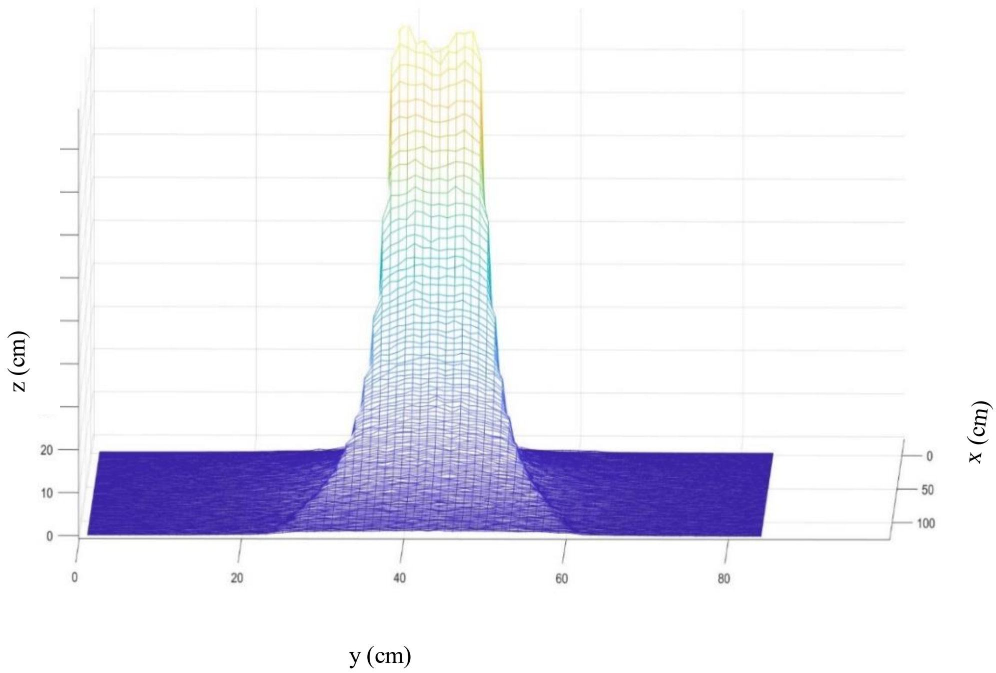

Figure4.10. *3D dose distribution of the FF beam obtained in water phantom using DOSXYZnrc for 40x40 cm^2 FS.*

5.4.1.Surface Dose

Surface dose refers to the radiation dose received by a patient's skin or by the phantom surface. The surface dose is significant in RT, and it is vital to be considered as it can impact the skin. The potential effects on the skin layer can vary in severity depending on the dose received by the skin surface. These effects can range from minor, like erythema or epilation, to more severe complications, such as desquamation or necrosis. The beam quality heavily influences the surface dose due to low-energy photons within the beam. To enhance the RT outcome, it is imperative to reduce the dose received by the skin while concurrently increasing the dose delivered to the tumor, thereby achieving improved tumor coverage.

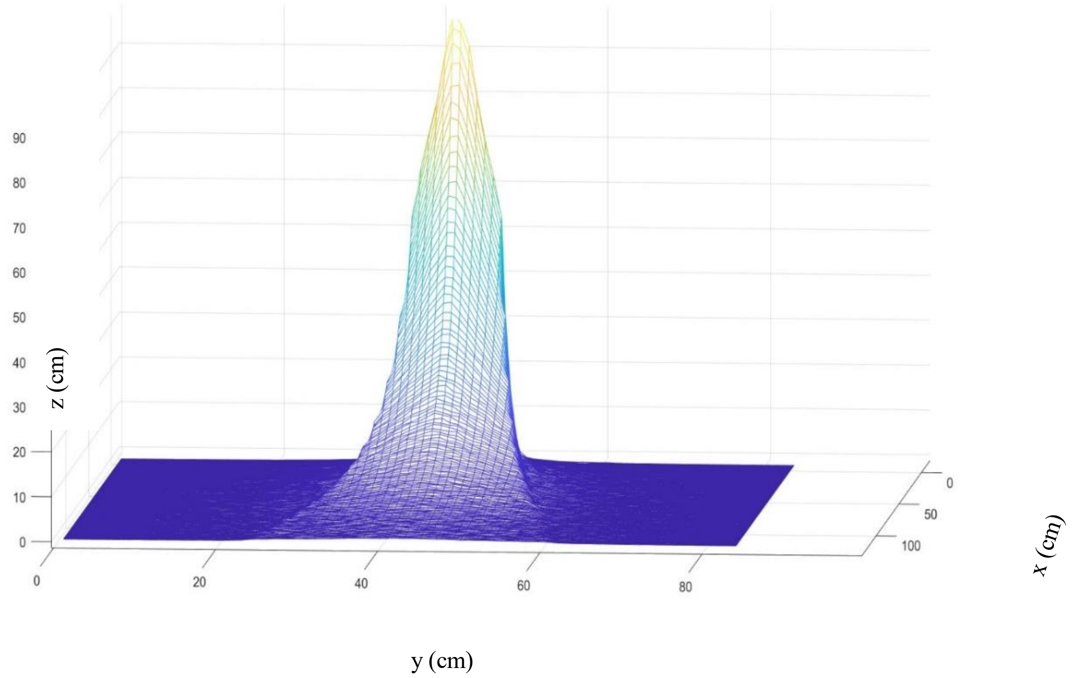

Figure4.11 *3D dose distribution of the FFF beam obtained in water phantom using DOSXYZnrc for 40x40 cm^2 FS.*

5.4.2.Surface dose of the FFF beam

Figure 4.12 shows the PDD curves of the FFF and the FF beams for the open field size (40x40 cm^2). The PDD curves were normalized to the maximum dose and analyzed for all beam configurations on the CA of a water phantom. The figure shows that the surface dose in the FFF beam is 5% higher than the FF beam. This observation is reported widely in literature reviews. Assalmi, M., & Diaf, E. Y. studied a 6 MV photon beam of Elekta Synergy linac using MC simulations and validated the results by experimental measurements in a water phantom. They found that the surface dose of the FFF beam is higher by 10 % for the 3x3, 5x5, and 10x10 cm^2 irradiation fields [60]. Also, Kajaria, A. et al. studied a 6 MV photon beam of the Varian Clinic 600 linac operated with and without a flattening filter using MC simulations and concluded that the surface doses were higher for the FFF beam by almost 6.8% [62] . An experimental study conducted by Shende et al. used a 6MV and 10MV photon beam and measured the surface dose with two different chambers, showed that the FFF beam had a higher surface dose with both chambers; also found that the increase in the surface dose using 10 MV photon beam is higher than using 6 MV with both chambers [30].

The increase in the surface dose in the FFF beam is because of low-energy photons and electron contamination. These photons have a low penetrating power, so they deposit their energy near the surface. In contrast, high-energy photons have a high penetrating power and deposit their energy deeper in the medium. This explanation is found in many studies. Kajaria A. et al. explained the increase in the surface dose in the study to more contamination electrons and low-energy photons in the beam [62]. Moreover, Mohammedet al. studied 6 MV photon beams using an MC simulation. They reported that surface doses were higher for the FFF beam due to more contamination electrons and low-energy photons in the beam [26].

5.4.2.1 The dependence of the surface dose on the FS

The variation in surface dose with FS for the FF and FFF beams is shown in Figure 4.13. The figures show that the surface dose increases linearly with FS for FF and FFF beams. However, the FFF beam shows less surface dose dependence on the FS. The surface dose results from electron contamination and low-energy photons. Figure 4.14 and Figure 4.15 demonstrate the effect of the electron contamination on the surface dose. Table 4.5 presents the numerical values of the surface dose for both the total PDD and the PDD without electron contamination. The impact of electron contamination is more apparent in the FF than in the FFF beam. Electron contamination amounts vary based on parameters such as field size, beam energy, and materials encountered in the beam's path. Removing the flattening filter reduces contamination electrons and increases the low-energy photons, as the filter also functions as a beam hardener. The FF beam exhibits a harder spectrum as it passes through the flattening filter. Consequently, it includes fewer low-energy photons and more contaminated electrons. In contrast, the FFF beam has a higher proportion of low-energy photons due to the absence of a flattening filter and less contaminated electrons. In the case of larger field sizes, more contamination electrons reach the surface as the primary beam interacts with a more significant surface area of the collimator and the air medium between the collimator and the phantom. The relationship between field size and surface dose increase is a widely recognized effect. This effect is mainly caused by electron contamination. Thus, removing the filter has the main benefit of reducing the variation of surface doses across different field sizes. The decrease in electron contamination results in FFF beams demonstrating significantly less surface dose variation with field size than FF beams.

Figure4.12. *PDD curves of the FF and FFF beams for the open field size (40x40 cm^2). Upright an inset for the surface dose from 0.25 to 0.35 cm*

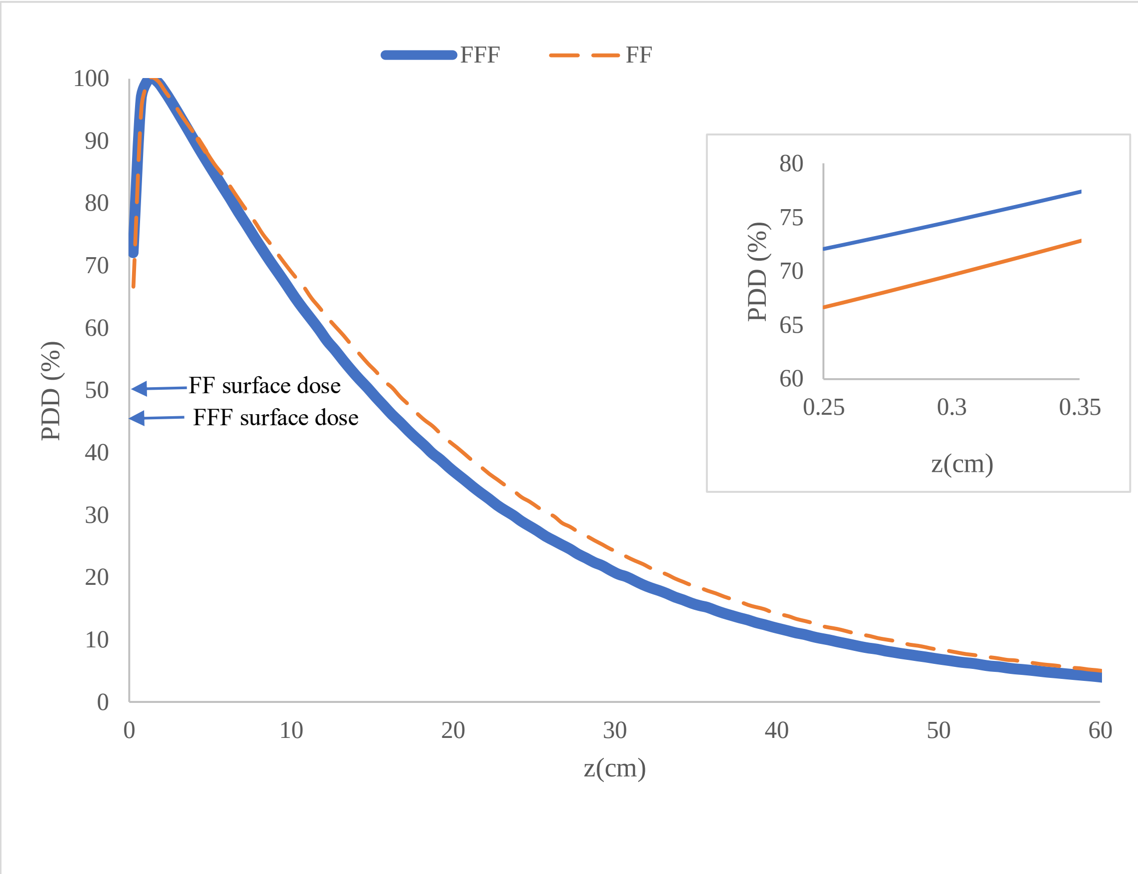

5.4.2.2.The dependence of the surface dose on the FS

The variation in surface dose with FS for the FF and FFF beams is shown in Figure 4.13. The figures show that the surface dose increases linearly with FS for FF and FFF beams. However, the FFF beam shows less surface dose dependence on the FS. The surface dose results from electron contamination and low-energy photons. Figure 4.14 and Figure 4.15 demonstrate the effect of the electron contamination on the surface dose. Table 4.5 presents the numerical values of the surface dose for both the total PDD and the PDD without electron contamination. The impact of electron contamination is more apparent in the FF than in the FFF beam. Electron contamination amounts vary based on parameters such as field size, beam energy, and materials encountered in the beam's path. Removing the flattening filter reduces contamination electrons and increases the low-energy photons, as the filter also functions as a beam hardener. The FF beam exhibits a harder spectrum as it passes through the flattening filter. Consequently, it includes fewer low-energy photons and more contaminated electrons. In contrast, the FFF beam has a higher proportion of low-energy photons due to the absence of a flattening filter and less contaminated electrons. In the case of larger field sizes, more contamination electrons reach the surface as the primary beam interacts with a more significant surface area of the collimator and the air medium between the collimator and the phantom. The relationship between field size and surface dose increase is a widely recognized effect. This effect is mainly caused by electron contamination. Thus, removing the filter has the main benefit of reducing the variation of surface doses across different field sizes. The decrease in electron contamination results in FFF beams demonstrating significantly less surface dose variation with field size than FF beams.

Many authors have investigated the effects of changing FS on the surface dose. For example, Cashmore, J. conducted an experimental investigation utilizing an Elekta Synergy linac equipped with 6MV and 10MV photon beams. The study found that as the FS increases, the surface dose will also increase, and most of this change is caused by electron contamination [63]. Chegeni, N. et al. did a study to review the sources of electron contamination and measurement based on dosimetry and simulations for RT and to investigate factors to reduce contamination reduction. Their study found that an increase in electron contamination results from using a flattering filter, a larger field size, a prosstudy in the patient's body, and a rise in photon energy [64].

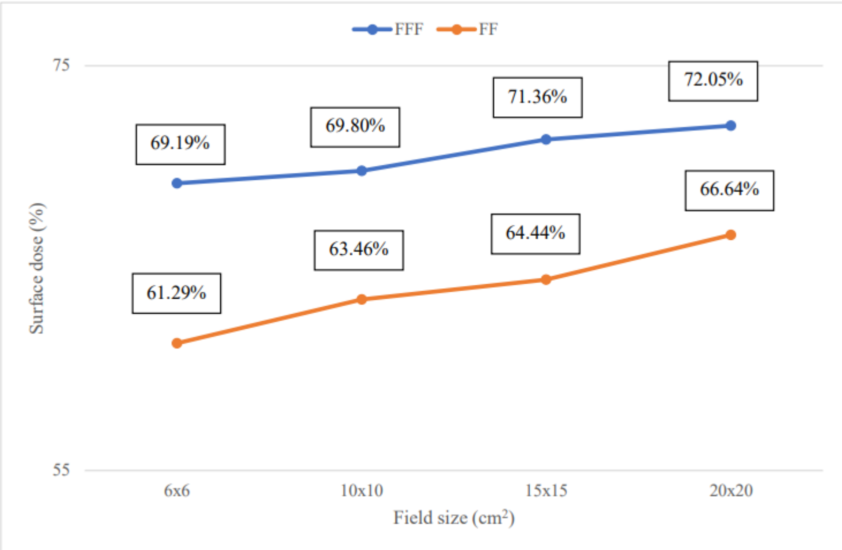

Figure 4.13 Surface dose as a function of field size.

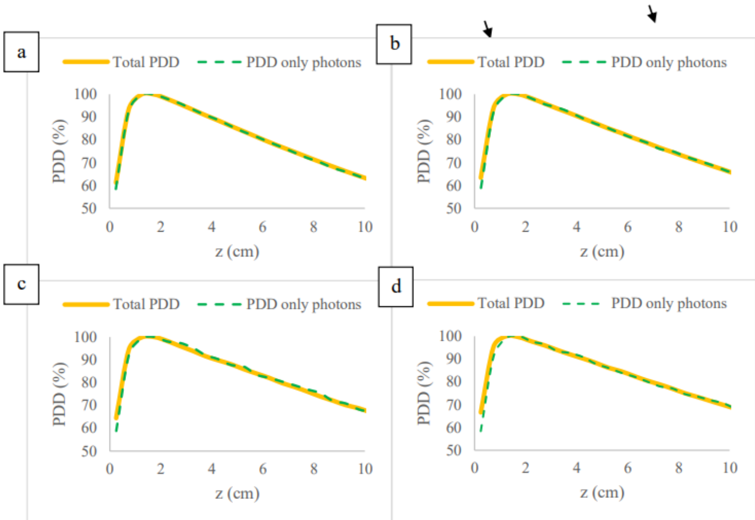

Figure4.14. Total PDD and PDD withot electron contamination of the FF beam for a. 6x6 cm^2, b.10x10 cm^2, c. 15x15 cm^2, d. 20x20 cm^2.

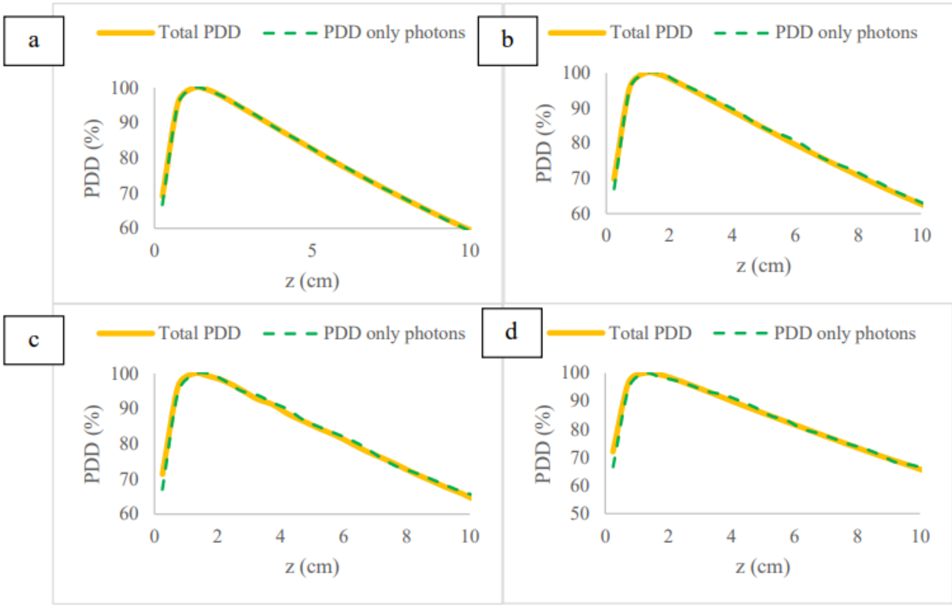

Figure4.15. *Total PDD and PDD without electron contamination of the FFF beam for a. 6x6 cm², b. 10x10 cm², c. 15x15 cm² d.20x20 cm² field sizes.*

Table4.5. *Percentage of surface dose with and without electron contamination for field sizes 6x6 cm²,10x10 cm², 15x15 cm², and 20x20 cm².*

Field size (cm²)	Surface dose (%) -Total PDD-		Surface dose (%) -PDD without electron contamination-	
	FF	FFF	FF	FFF
6x6	61.33646	69.19037	58.53825	66.70495
10x10	63.46465	69.80568	58.95519	67.00216
15x15	64.44191	71.36624	58.76366	67.0423
20x20	66.56376	72.05294	58.35898	66.62199

Surface dose of the FFF beam with low-z material filters

Low-z material filters improve the RT outcomes of the FFF beam by reducing the surface dose while keeping the dose rate higher than the FF beam. Figure 4.16 shows the effect of Al and steel filters on the PDD curve of the FFF beam. An inset for the surface dose is presented in the corner of Figure 4.16. Adding filters from low-z material to the beam's path of the FFF beam improves the skin-sparing effect as the surface dose decreases. Furthermore, the dose increased at a depth greater than D_{max}, resulting in better coverage for treating the tumor at a depth. The surface dose decreased by around 14.7% and 18.02%, while the dose at a depth of 10 cm increased by approximately 23% and 26% for Al and steel, respectively. The steel filter absorbs more low-energy photons, improving the FFF beam's RT outcomes more than the Al filter.

6. CONCLUSION

To summarize, we present and discuss the study's findings in this chapter. First, The FFF beam is softer than the FF beam. Moreover, the surface dose increased in the FFF beam due to more low-energy photons contributing to the beam. Also, The FFF beam has a higher photon energy fluence, reflecting a higher dose rate than the Flattened beam. As the FFF beam has a high dose rate, we will benefit from having a shorter treatment duration. Reducing the treatment duration helps in patient comfort. Secondly, filters made from low-z material with the FFF beam will harden the beam as the filters will absorb a portion of low-energy photons from the beam. Additionally, the surface dose will reduced also. The FFF beam's dose rate will reduce when we use these filters but still have a higher dose rate than the FF beam. However, using filters from low-z material improves the therapeutic outcomes of the FFF beam by reducing the surface dose while maintaining a high dose rate.

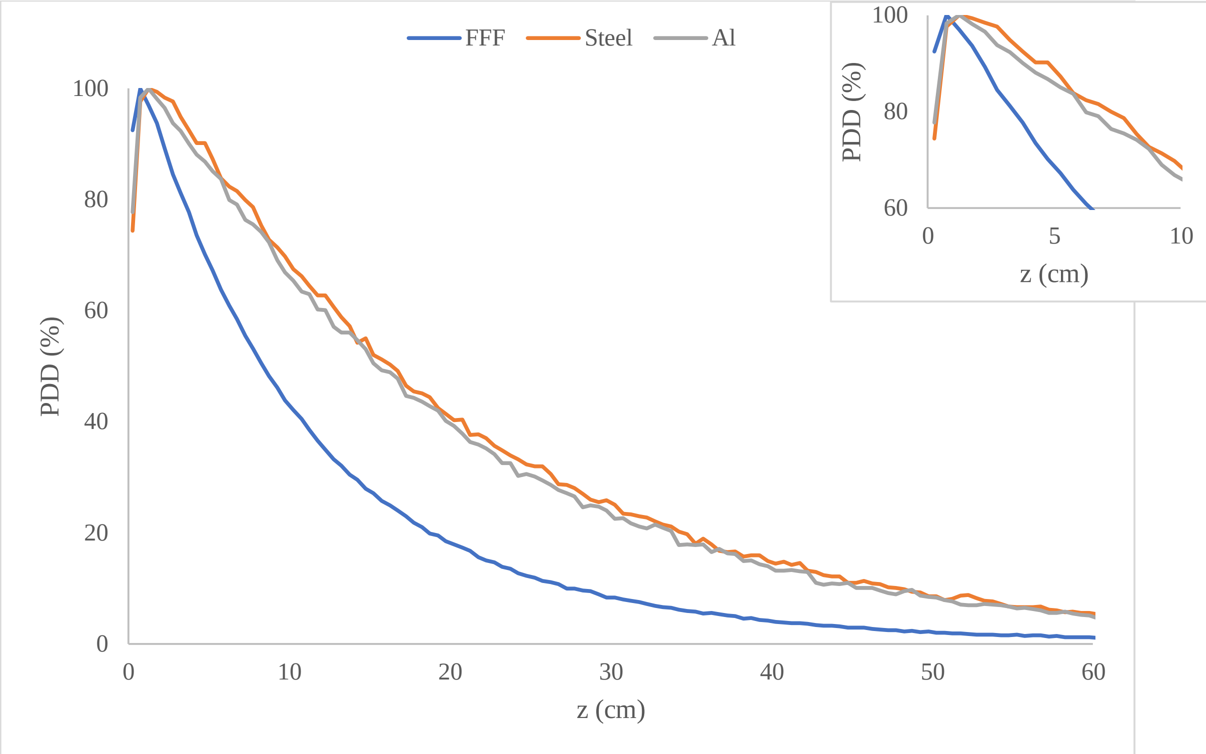

Figure4.16. *PDD curves of the FFF beam with and without low-z material filter***,** *upright the graph an inset for the surface dose.*

Future work

While further research is needed to determine weather the current results are generally applicable, the previously described studies provided valuable understanding of novel strategies for enhancing the therapeutic outcomes of the FFF beam through the incorporative of low-z material filters. However, the study recommends the following:

- Investigating the impact of aluminum and steel on the small field size dosimetry smaller than 6x6 cm^2.
- Investigating the impact of another low-z materials eg:- pure or composite materials.
- Simulate the dose distribution in an inhomogeneous phantom.
- Further studies into dosimetric characteristics, such as build-up dosage and penumbra, is recommended.
- Implement this study experimentally and compare the findings with the simulation results.

REFERENCES

[1] S. Sharma, “Unflattened photon beams from the standard flattening filter free accelerators for radiotherapy: Advantages, limitations and challenges,” *J Med Phys*, vol. 36, no. 3, p. 123, 2011, doi: 10.4103/0971-6203.83464.

[2] A. Sigamani *et al.*, “Surface dose measurements and comparison of unflattened and flattened photon beams,” *J Med Phys*, vol. 41, no. 2, p. 85, 2016, doi: 10.4103/0971-6203.181648.

[3] S. Lang *et al.*, “Clinical application of flattening filter free beams for extracranial stereotactic radiotherapy,” *Radiotherapy and Oncology*, vol. 106, no. 2, pp. 255–259, Feb. 2013, doi: 10.1016/j.radonc.2012.12.012.

[4] J.-Y. Lu, J. Zheng, W.-Z. Zhang, and B.-T. Huang, “Flattening Filter-Free Beams in Intensity-Modulated Radiotherapy and Volumetric Modulated Arc Therapy for Sinonasal Cancer,” *PLoS One*, vol. 11, no. 1, p. e0146604, Jan. 2016, doi: 10.1371/journal.pone.0146604.

[5] M. Lederman, “The early history of radiotherapy: 1895–1939,” *International Journal of Radiation Oncology*Biology*Physics*, vol. 7, no. 5, pp. 639–648, May 1981, doi: 10.1016/0360-3016(81)90379-5.

[6] S. Gianfaldoni, R. Gianfaldoni, U. Wollina, J. Lotti, G. Tchernev, and T. Lotti, “An Overview on Radiotherapy: From Its History to Its Current Applications in Dermatology.,” *Open Access Maced J Med Sci*, vol. 5, no. 4, pp. 521–525, Jul. 2017, doi: 10.3889/oamjms.2017.122.

[7] R. Baskar, K. A. Lee, R. Yeo, and K.-W. Yeoh, “Cancer and Radiation Therapy: Current Advances and Future Directions,” *Int J Med Sci*, vol. 9, no. 3, pp. 193–199, 2012, doi: 10.7150/ijms.3635.

[8] F. M. Khan and J. P. Gibbons, *Khan’s the physics of radiation therapy*. Lippincott Williams & Wilkins, 2014.

[9] D. , & W. P. C. Greene, *Linear accelerators for radiation therapy*. 1997.

[10] C. L. Hartmann Siantar *et al.*, “Description and dosimetric verification of the Monte Carlo dose calculation system for photon beams incident on a water phantom,” *Med Phys*, vol. 28, no. 7, pp. 1322–1337, Jul. 2001, doi: 10.1118/1.1381551.

[11] F. Verhaegen and J. Seuntjens, “Monte Carlo modelling of external radiotherapy photon beams,” *Phys Med Biol*, vol. 48, no. 21, pp. R107–R164, Nov. 2003, doi: 10.1088/0031-9155/48/21/R01.

[12] E. Bezak and K. Quach, “Simulation of the Transmitted Dose in an EPID Using a Monte Carlo Method Thuc M Pham,” 2009.

[13] P. , N. A. , & R. J. C. Mayles, *Handbook of Radiotherapy Physics*. CRC Press, 2007. doi: 10.1201/9781420012026.

[14] M. Ariff and J. Sidek, “MONTE CARLO INVESTIGATIONS OF RADIOTHERAPY BEAMS: STUDIES OF CONVENTIONAL, STEREOTACTIC AND UNFLATTENED BEAMS,” 2010.

[15] M. Constantin *et al.*, “Modeling the TrueBeam linac using a CAD to Geant4 geometry implementation: Dose and IAEA-compliant phase space calculations,” *Med Phys*, vol. 38, no. 7, pp. 4018–4024, Jun. 2011, doi: 10.1118/1.3598439.

[16] D. Sardari, R. Maleki, H. Samavat, and A. Esmaeeli, “Measurement of depth-dose of linear accelerator and simulation by use of Geant4 computer code,” *Reports of Practical Oncology & Radiotherapy*, vol. 15, no. 3, pp. 64–68, May 2010, doi: 10.1016/j.rpor.2010.03.001.

[17] International Nuclear Atlantic Conference (2013 : Recife), *The benefits of nuclear technology for social inclusion*. Associação Brazilieira de Energia Nuclear, 2013.

[18] T. Tuğrul, “Effect of different target materials of LINAC head on photon spectrum,” *J Radiat Res Appl Sci*, vol. 14, no. 1, pp. 204–209, Dec. 2021, doi: 10.1080/16878507.2021.1921964.

[19] P. Weber, J.-L. Vuilleumier, G. Guibert, and C. Tamburella, “Linac activation of radioisotopes and underground gammaspectrometric analyses.” [Online]. Available: http://ssrpm.ch/publications-and

[20] J. Cashmore, M. Ramtohul, and D. Ford, “Lowering Whole-Body Radiation Doses in Pediatric Intensity-Modulated Radiotherapy Through the Use of Unflattened Photon Beams,” *International Journal of Radiation Oncology*Biology*Physics*, vol. 80, no. 4, pp. 1220–1227, Jul. 2011, doi: 10.1016/j.ijrobp.2010.10.002.

[21] Y. Yan *et al.*, “Dosimetric differences in flattened and flattening filter-free beam treatment plans,” *J Med Phys*, vol. 41, no. 2, p. 92, 2016, doi: 10.4103/0971-6203.181636.

[22] Y. Wang, M. K. Khan, J. Y. Ting, and S. B. Easterling, “Surface Dose Investigation of the Flattening Filter-Free Photon Beams,” *International Journal of Radiation Oncology*Biology*Physics*, vol. 83, no. 2, pp. e281–e285, Jun. 2012, doi: 10.1016/j.ijrobp.2011.12.064.

[23] Y. Huang, R. Alfredo Siochi, and J. E. Bayouth, “Dosimetric properties of a beam quality-matched 6 MV unflattened photon beam,” *J Appl Clin Med Phys*, vol. 13, no. 4, pp. 71–81, 2012, doi: 10.1120/jacmp.v13i4.3701.

[24] D. Georg, T. Knöös, and B. McClean, “Current status and future perspective of flattening filter free photon beams,” *Med Phys*, vol. 38, no. 3, pp. 1280–1293, Feb. 2011, doi: 10.1118/1.3554643.

[25] O. N. Vassiliev, U. Titt, F. Pönisch, S. F. Kry, R. Mohan, and M. T. Gillin, “Dosimetric properties of photon beams from a flattening filter free clinical accelerator,” *Phys Med Biol*, vol. 51, no. 7, pp. 1907–1917, Apr. 2006, doi: 10.1088/0031-9155/51/7/019.

[26] M. Mohammed, E. Chakir, H. Boukhal, S. Mroan, and T. El Bardouni, “Evaluation of the dosimetric characteristics of 6 MV flattened and unflattened photon beam,” *J King Saud Univ Sci*, vol. 29, no. 3, pp. 371–379, Jul. 2017, doi: 10.1016/j.jksus.2016.09.008.

[27] G. Reggiori *et al.*, “Can volumetric modulated arc therapy with flattening filter free beams play a role in stereotactic body radiotherapy for liver lesions? A volume-based analysis,” *Med Phys*, vol. 39, no. 2, pp. 1112–1118, Feb. 2012, doi: 10.1118/1.3679858.

[28] A. Detappe, P. Tsiamas, W. Ngwa, P. Zygmanski, M. Makrigiorgos, and R. Berbeco, “The effect of flattening filter free delivery on endothelial dose enhancement with gold nanoparticles,” *Med Phys*, vol. 40, no. 3, p. 031706, Feb. 2013, doi: 10.1118/1.4791671.

[29] O. N. Vassiliev, U. Titt, S. F. Kry, F. Pönisch, M. T. Gillin, and R. Mohan, "Monte Carlo study of photon fields from a flattening filter-free clinical accelerator," *Med Phys*, vol. 33, no. 4, pp. 820–827, Mar. 2006, doi: 10.1118/1.2174720.

[30] R. Shende, G. Gupta, G. Patel, and S. Kumar, "Commissioning of TrueBeam; Medical Linear Accelerator: Quantitative and Qualitative Dosimetric Analysis and Comparison of Flattening Filter (FF) and Flattening Filter Free (FFF) Beam," *Int J Med Phys Clin Eng Radiat Oncol*, vol. 05, no. 01, pp. 51–69, 2016, doi: 10.4236/ijmpcero.2016.51006.

[31] P. Andreo, "Monte Carlo techniques in medical radiation physics," *Phys Med Biol*, vol. 36, no. 7, pp. 861–920, Jul. 1991, doi: 10.1088/0031-9155/36/7/001.

[32] K. Jabbari, "Review of fast Monte Carlo codes for dose calculation in radiation therapy treatment planning," *J Med Signals Sens*, vol. 1, no. 1, p. 73, 2011, doi: 10.4103/2228-7477.83522.

[33] I. J. Chetty *et al.*, "Report of the AAPM Task Group No. 105: Issues associated with clinical implementation of Monte Carlo-based photon and electron external beam treatment planning," *Med Phys*, vol. 34, no. 12, pp. 4818–4853, Nov. 2007, doi: 10.1118/1.2795842.

[34] I. J. Chetty *et al.*, "Report of the AAPM Task Group No. 105: Issues associated with clinical implementation of Monte Carlo-based photon and electron external beam treatment planning," *Med Phys*, vol. 34, no. 12, pp. 4818–4853, Nov. 2007, doi: 10.1118/1.2795842.

[35] W. R. Nelson and Y. Namitot, "THE EGS4 CODE SYSTEM: SOLUTION OF GAMMA-RAY AND ELECTRON TRANSPORT PROBLEMS*," 1985.

[36] I. Kawrakow, "The EGSnrc code system, Monte Carlo simulation of electron and photon transport," 2001.

[37] Judith F, "MCNP TM-A General Monte Carlo N-Particle Transport Code Version 4C," 2000.

[38] S. , A. J. , A. K. A. , A. J. , A. H. , A. P. , . . . & G. Collaboration. Agostinelli, "Geant4—a simulation toolkit," 2003.

[39] D. W. O. Rogers, B. Walters, and I. Kawrakow, "BEAMnrc Users Manual," 2023.

[40] C.-M. Ma and D. W. O. Rogers, "BEAMDP Users Manual," 2023.

[41] B. Walters, I. Kawrakow, and D. W. O. Rogers, "DOSXYZnrc Users Manual," 2023.

[42] M. Vimolnoch, I. I. N. Ayuthaya, S. Kingkaew, and S. Oonsiri, "Evaluation of the Varian TrueBeam™ 6 MV phase-space files for the Monte Carlo simulation in small field dosimetry," *Journal of Associated Medical Sciences*, vol. 55, no. 3. Faculty of Associated Medical Sciences, Chiang Mai University, pp. 26–35, Sep. 01, 2022. doi: 10.12982/jams.2022.021.

[43] D. M. Ghemiş and L. G. Marcu, "Progress and prospects of flattening filter free beam technology in radiosurgery and stereotactic body radiotherapy," *Crit Rev Oncol Hematol*, vol. 163, p. 103396, Jul. 2021, doi: 10.1016/j.critrevonc.2021.103396.

[44] O. N. Vassiliev, C. B. Peterson, J. Y. Chang, and R. Mohan, "Using FFF beams to improve the therapeutic ratio of lung SBRT," *J Radiother Pract*, vol. 20, no. 4, pp. 419–425, Dec. 2021, doi: 10.1017/S1460396920000576.

[45] D. Pokhrel, M. Halfman, and L. Sanford, "FFF-VMAT for SBRT of lung lesions: Improves dose coverage at tumor-lung interface compared to flattened beams," *J Appl Clin Med Phys*, vol. 21, no. 1, pp. 26–35, Jan. 2020, doi: 10.1002/acm2.12764.

[46] A. , S. R. , & E. M. R. C. Zeghari, "Monte Carlo study of a free flattening filter to increase surface dose on 12 MV photon beam," *International Journal of Radiation Research*, 2020.

[47] A. Sigamani *et al.*, "Surface dose measurements and comparison of unflattened and flattened photon beams," *J Med Phys*, vol. 41, no. 2, p. 85, 2016, doi: 10.4103/0971-6203.181648.

[48] J.-Y. Lu, J. Zheng, W.-Z. Zhang, and B.-T. Huang, "Flattening Filter-Free Beams in Intensity-Modulated Radiotherapy and Volumetric Modulated Arc Therapy for Sinonasal Cancer," *PLoS One*, vol. 11, no. 1, p. e0146604, Jan. 2016, doi: 10.1371/journal.pone.0146604.

[49] M. F. Belosi *et al.*, "Monte Carlo simulation of TrueBeam flattening-filter-free beams using Varian phase-space files: Comparison with experimental data," *Med Phys*, vol. 41, no. 5, p. 051707, Apr. 2014, doi: 10.1118/1.4871041.

[50] K. Javedan *et al.*, "Monte Carlo comparison of superficial dose between flattening filter free and flattened beams," *Physica Medica*, vol. 30, no. 4, pp. 503–508, Jun. 2014, doi: 10.1016/j.ejmp.2014.03.001.

[51] M. Jaafar Sidek, "MONTE CARLO INVESTIGATIONS OF RADIOTHERAPY BEAMS: STUDIES OF CONVENTIONAL, STEREOTACTIC AND UNFLATTENED BEAMS.," University of Birmingham, 2010.

[52] Roberto Capote, "Phase-space database for external beam radiotherapy."

[53] C. Moler, "MATLAB Users' Guide," 1980. [Online]. Available: http://www.mathworks.com/company/clevebio.shtml

[54] IAEA, “https://www-nds.iaea.org/phsp/phsp.htmlx.”

[55] Varian, “Home | Varian. (n.d.). Home | Varian. https://www.varian.com/,” Varian.

[56] M. F. Belosi *et al.*, “Monte Carlo simulation of TrueBeam flattening-filter-free beams using Varian phase-space files: Comparison with experimental data,” *Med Phys*, vol. 41, no. 5, p. 051707, Apr. 2014, doi: 10.1118/1.4871041.

[57] T. Teke, C. Duzenli, A. Bergman, F. Viel, P. Atwal, and E. Gete, “Monte Carlo validation of the TrueBeam 10XFFF phase-space files for applications in lung SABR,” *Med Phys*, vol. 42, no. 12, pp. 6863–6874, Nov. 2015, doi: 10.1118/1.4935144.

[58] M. Mohammed *et al.*, “Dosimetric Properties of the Field Sizes of 12MV Photon Beams: A Monte Carlo Study,” *Journal of Nuclear and Particle Physics*, vol. 5, pp. 52–57, Jun. 2015, doi: 10.5923/j.jnpp.20150503.02.

[59] A. Mesbahi, “Dosimetric characteristics of unflattened 6MV photon beams of a clinical linear accelerator: A Monte Carlo study,” *Applied Radiation and Isotopes*, vol. 65, no. 9, pp. 1029–1036, Sep. 2007, doi: 10.1016/j.apradiso.2007.04.023.

[60] M. Assalmi and E. Y. Diaf, “Monte Carlo Simulation of Surface Dose and Dose Rate in 6MV-FFF Beams,” *Moscow University Physics Bulletin*, vol. 76, no. S1, pp. S36–S51, Dec. 2021, doi: 10.3103/S0027134922010027.

[61] T. Jaruthien *et al.*, “Flattening filter free stereotactic body radiation therapy for lung tumors: outcomes and predictive factors,” *Transl Cancer Res*, vol. 10, no. 2, pp. 571–580, Feb. 2021, doi: 10.21037/tcr-20-3174.

[62] A. Kajaria, N. Sharma, S. Sharma, S. Pradhan, A. Mandal, and Lalit. M. Aggarwal, “Study of the dosimetric properties of an unflattened 6-MV photon beam by using the BEAMnrc code,” *Journal of the Korean Physical Society*, vol. 69, no. 4, pp. 657–665, Aug. 2016, doi: 10.3938/jkps.69.657.

[63] J. Cashmore, “Surface dose variations in 6 and 10 MV flattened and flattening filter-free (FFF) photon beams,” *J Appl Clin Med Phys*, vol. 17, no. 5, pp. 293–307, Sep. 2016, doi: 10.1120/jacmp.v17i5.6284.

[64] N. Chegeni, F. Rahim, M. Tahmasbi, Z. Farzanegan, and S. K. Hosseini, “Measurement and Calculation of Electron Contamination for Radiotherapy Photon Mode,” *Jundishapur Journal of Health Sciences*, vol. 13, no. 1, Jun. 2021, doi: 10.5812/jjhs.115067.

Citation: *Hadeel Mohammed Saleh Alfrihidi & Dr. Hussein Abdulrahman Albarakaty, " The Effect of Low Atomic Number Fillters on the Flattening Filters free photon Beamin in Radiotherapy" International Journal of Advanced Research in Physical Science (IJARPS), vol 11, no. 12, pp. 3-31, 2024.*